Chem Soc Rev

REVIEW ARTICLE

View Article Online
View Journal | View Issue

Cite this: *Chem. Soc. Rev.*, 2022, **51**, 4465

Porous organic polymers in solar cells†

Tianyi Zhang, [a] Vasilis G. Gregoriou,[bc] Nicola Gasparini [a] and Christos L. Chochos *[bd]

Owing to their unique porosity and large surface area, porous organic polymers (POPs) have shown their presence in numerous novel applications. The tunability and functionality of both the pores and backbone of the material enable its suitability in photovoltaic devices. The porosity induced host–guest configurations as well as periodic donor–acceptor structures benefit the charge separation and charge transfer in photophysical processes. The role of POPS in other critical device components, such as hole transporting layers and electrodes, has also been demonstrated. Herein, this review will primarily focus on the recent progress made in applying POPs for solar cell device performance enhancement, covering organic solar cells, perovskite solar cells, and dye-sensitized solar cells. Based on the efforts in recent years in unraveling POP's photophysical process and its relevance with device performances, an in-depth analysis will be provided to address the gradual shift of attention from an entirely POP-based active layer to other device functional components. Combining the insights from device physics, material synthesis, and microfabrication, we aim to unfold the fundamental limitations and challenges of POPs and shed light on future research directions.

Received 11th February 2022

DOI: 10.1039/d2cs00123c

rsc.li/chem-soc-rev

[a] *Department of Chemistry and Centre for Processable Electronics, Imperial College London, W12 0BZ, UK*
[b] *Advent Technologies SA, Stadiou Street, Platani, Rio, Patras 26504, Greece. E-mail: cchochos@advent.energy, chochos@eie.gr*
[c] *National Hellenic Research Foundation, 48 Vassileos Constantinou Avenue, Athens, 11635, Greece*
[d] *Institute of Chemical Biology, National Hellenic Research Foundation, 48 Vassileos Constantinou Avenue, Athens 11635, Greece*

† Electronic supplementary information (ESI) available. See DOI: https://doi.org/10.1039/d2cs00123c

1 Introduction

Ever since the emergence of covalently-bonded porous organic polymers (POPs), abundant research has been dedicated to exploiting their intrinsic porosity and high surface area which are attributed to their unique interconnected backbone structure. Along with their electrical functionalities as well as chemical and thermal stabilities,[1] POPs have shown their presence in a wide range of applications including gas

Tianyi Zhang

Tianyi Zhang finished his master's at the Center for Processable Electronics, Imperial College London in 2021. With an electrical engineering bachelor's degree from Shanghai Tech University, his wide interests in the area of flexible and organic electronics motivated him to perform research at UC Berkeley, KAUST solar center, and Imperial. While devoted to exploring fundamental physics, he also strives to accelerate the device application and commercialization process with his interdisciplinary background. He is now a PhD candidate at Technische Universität Dresden under the supervision of Prof. Karl Leo.

Vasilis G. Gregoriou

Dr Vasilis Gregoriou has been the Chairman and CEO of Advent Technologies Holdings Inc. since its inception and Chairman of the Board at the National Hellenic Research Foundation (NHRF) in Athens Greece. His research activities extend over a wide area of subjects in the renewable energy space that include the areas of flexible photovoltaics based on organic semiconductors, optically active materials based on conjugated oligomers and polymer nanocomposites. Dr Gregoriou has more than 25 years of experience in the US market. He holds a PhD in Physical Chemistry from Duke University and he has attended the MBA program at Northeastern University.

adsorption,[2–4] sensing,[5–7] photocatalysis,[8–10] energy storage,[11–13] and drug delivery.[14–16] Typical POPs are comprised of different and periodic monomeric building blocks to form a network, namely linkers and nodes (knots) that provide rigidity and functionality to various topological designs. Given the specific heteroatom that is involved during the linkage formation, boronic esters as well as boroxine can be formed in the case of boron atoms,[1,17] whereas imine, azine, and imide are utilized in the case of nitrogen atoms.[18–20] These linkages provide strong covalent bonds to connect building blocks. Depending on the degree of crystallinity, POPs can further be classified as amorphous and crystalline analogs.[21] The former mainly includes the concept of hyper-crosslinked polymers (HCPs),[22] conjugated microporous polymers (CMPs),[23] porous aromatic frameworks (PAFs),[24] and polymers with intrinsic microporosity (PIM).[25] The latter predominantly belong to covalent organic frameworks (COFs).[26]

In order to realize desired pore sizes, crystallinity, and morphology for effective functionality, synthetic control for different frameworks and topologies is of prime importance for the targeted polymer. Accompanied by numerous burgeoning post-synthetic modification methods,[27–30] POPs endow a powerful platform for attaining primary and high-order structures as well as tunable end products. It is worth noting that structural rigidity largely limits the solubility of POPs in common solvents, which greatly restrains its processability.[31–33] For organic semiconductor materials, a π-conjugated backbone renders the electronic foundation for charge delocalization. However, the geometric properties of POPs determine the interplay between rigidity and conjugation, remaining a formidable hurdle for optimized design.[34] A variety of polymerization techniques have been adopted to achieve high-yield and topologically guided fine molecular structures, which include solvothermal,[35,36] mechanochemical,[37,38] ionothermal,[39,40] microwave,[41,42] on-substrate,[43,44] and other promising methods.[45,46] While some approaches produce insoluble crystals, others simultaneously produce thickness-controllable thin films by the end of synthesis[26,47] (*e.g. in situ* electro-polymerization[48]). In-depth analyses of POP synthesis strategies have been addressed in recent research.[23,26,49–51]

The intriguing porosities, tunable backbone, and topological advantages of POPs have attracted wide research interest in exploiting their versatility,[23,26,51–53] which instigated the connection between POPs and photovoltaics. The reported ultra-long charge carrier lifetime and efficient charge transport[23,26,33,50] demonstrated their great potential for promising photovoltaic devices. Photovoltaics (PV) has demonstrated its outstanding energy conversion ability to serve as a green energy resource to help human beings achieve zero-carbon emission. Generating electricity by harvesting solar energy, judicious design and in-depth understanding of photophysical properties play key roles in propelling the development of solar cell technology. Recent years have witnessed the emergence of perovskite solar cells (PSCs), with the highest record efficiency of 25.2% to date,[54] which is approaching the performance of single-crystalline silicon.[55] Exploiting abundantly available elements as the active layer for PSCs, researchers also explore alternative non-toxic options like bismuth[56] and antimony[57] for a greener future. As more tunable and highly luminescent small fullerene acceptors become available, organic solar cells (OSCs) also demonstrate promising efficiency which approaches 20%.[58] Owing to facile processing and tunability of the organic materials, OSCs obtain unique properties of low cost, flexibility, and scalability which mark their competitiveness in the commercial market. Dye-sensitized solar cells (DSSCs), on the other hand, have demonstrated outstanding performances under faint and artificial light conditions, which promotes their indoor applications.[59–61] Since the proof-of-concept of employing POPs in PV reported in 2013,[62] enormous effort has been dedicated to using POPs as the photoactive component. In addition to the incorporation in

Nicola Gasparini

Dr Nicola Gasparini received his BSc and MSc, in Chemistry and Organic Chemistry, and Photochemistry and Molecular Materials, respectively, from the University of Bologna, Italy. In 2017 he received his PhD from the Institute of Materials for Electronics and Energy Technology (i-MEET) at the Friedrich Alexander University Erlangen-Nürnberg (FAU) under the supervision of Professor Brabec. In September 2017, he joined the King Abdullah University of Science and Technology (KAUST) and since September 2019, he has been an academic researcher at Imperial College London. His research interests are in organic semiconductors, with focus on organic photovoltaics and photodetectors with over 100 publications.

Christos L. Chochos

Dr Christos Chochos holds a degree in Chemistry from the Chemistry Department of University of Patras and a MSc and a PhD from the Interdepartmental (Chemistry, Physics, Chemical Engineering, Materials Science and Engineering) program in Polymer Science and Technology of University of Patras, Greece. Now, he is a Senior Researcher at the Institute of Chemical Biology at the National Hellenic Research Foundation, Athens, Greece, and project manager at Advent Technologies SA. His research interests include the design, synthesis, and characterization of conjugated polymers for various optoelectronic and bioimaging applications.

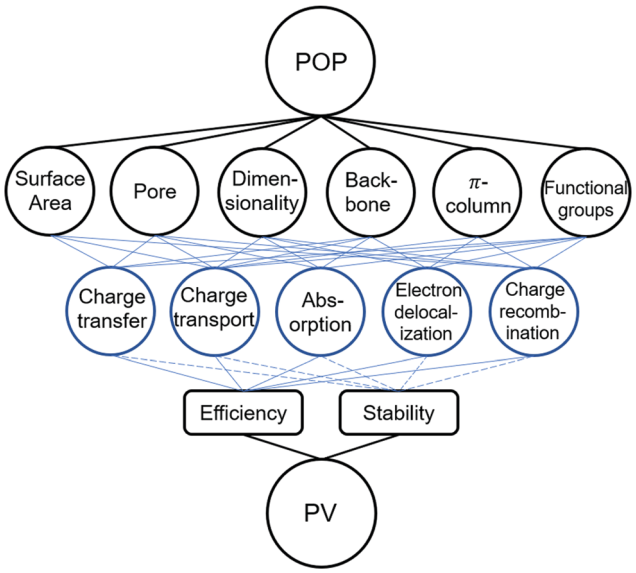

Scheme 1 POP properties' correlation with PV performance in terms of photophysical parameters. Dashed lines indicate that further research effort is needed to establish the relationship in the case of POPs.

the photoactive layer, multiple attempts were also made to employ POPs as the hole/electron transporting layer (HTL/ETL),[63–65] which further demonstrated the diversity and feasibility of POPs for PV technologies.

Herein, a holistic review is provided to unfold the potential POPs for PV application, specifically in the sub-category of OPVs, PSCs, and DSSCs (Scheme 1). To provide a systematic approach for further device improvement, detailed analyses from the aspect of fundamental photophysics to various device functionalities will be presented. Moreover, insights and perspective on long-term stability are also proposed to present an alternative strategy and focus to accelerate the commercialization of POP incorporated solar cells. Based on recent progress, we envisage to bring a multifaceted-engineering perspective to relate specific optoelectronic properties to critical device performance factors, which can justify the gradual shift from the active layer to other device functional components and shed light on design strategies for next-generation solar cells.

2 POP incorporation in photovoltaic technologies

Unlike their linear counterpart, which is comparably more susceptible to aggregation and charge localization due to its soft and brittle nature determined by its geometric kinetics, POPs establish their topological network through robust covalent bonds that help define the charge transport channel and thermal stability.[26,52,66,67] As higher dimension POP networks become available,[36,68–70] their unique structural advantage lays a thrilling foundation for isotropic multi-dimensional charge transport and transfer. From an optoelectronic point of view, it is of paramount importance to thoroughly establish comprehensive material characterization for advanced PV applications, which necessitates a fine condition of film/powder/solution formation.[23,26,53] Therefore, few photophysical studies were available to date compared to the enormous amount of progress in synthetic materials. These are mainly restricted by the insolubility and crystallinity issues of POPs, which is mainly due to the backbone rigidity, synthetic control, and processing conditions.[71,72] This thus explains why predominant research effort is focused on COFs, which require long-range order to retain more crystallinity than other categories. CMPs, albeit amorphous, win tremendous research attention due to their facile synthesis and adjustability.[23,73,74] For other classes of porous materials, either their stringent and inflexible synthetic conditions or the overall less crystalline feature with limited π-conjugation significantly hinders their optoelectronic applications. CTFs, for instance, bear outstanding merits due to the presence of a high amount of nitrogen, but their triazine ring synthesis drastically withholds their mass production and versatile applications.[9,75] PAFs, typically synthesized by Ullmann cross-coupling, face a high hurdle to realize large-scale and low-cost production.[76,77]

2.1 POP photophysical properties

The intriguing properties of POPs attract continuous research effort to implement them in not only the photoactive layer, but also in the ETL/HTL and electrolyte. Fig. 1 shows a summary of the power conversion efficiency (PCE) covering recent POP-incorporated solar cells. Detailed functionality of POPs in the devices and other key performances parameters are also tabulated in Table 1.

It is noteworthy that the number of POP-specific PV reports is astonishingly smaller than that of other POP applications.[23,52] It is evident from the figure that successful combination of POPs and perovskites has exhibited promising results over the last few years. The intrinsic hydrophobicity serves as perfect passivation for ambient species invasion, which promotes the device's long-term operation stability.[91] Its porous structure and tunable energy level can also effectively passivate those defect states for

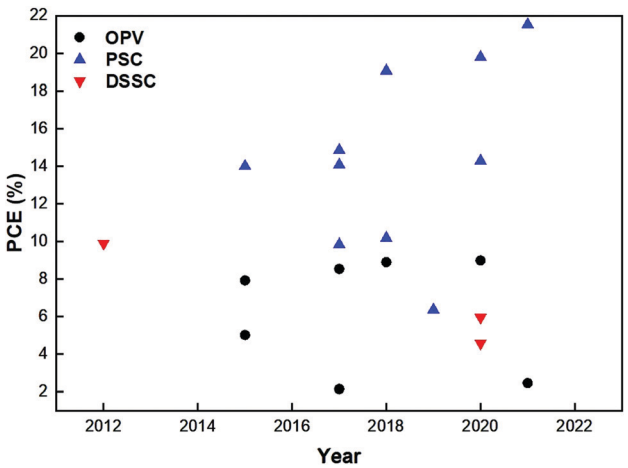

Fig. 1 Yearly power conversion efficiency (PCE) progress based on POP incorporated PV devices.

Table 1 Summary of specific key solar cell performance figure of merits for recent POP-incorporated PVs

PV type	Year	PCE (%)	FF (%)	J_{sc} (mA cm^{-2})	V_{oc} (V)	POP function	POP type	Ref.
OPV	2013	7.56	65.7	12.44	0.925	HTL	CMP	78
OPV	2015	5.02	68.2	10.05	0.732	AL (donor)	CMP	79
OPV	2016	7.93	63.5	16.12	0.775	ETL/HTL	—	63
OPV	2017	2.15	30	8.7	0.83	AL (acceptor)	—	80
OPV	2017	8.54	70.62	15.98	0.74	HTL	—	81
OPV	2018	8.9	70.64	16.14	0.78	HTL	CMP	64
OPV	2020	8.99	66.21	16.98	0.8	HTL	—	65
OPV	2021	2.46	38.68	7.95	0.8	AL (donor)	COF	82
Perovskite	2015	14	76.3	18.7	0.979	ETL	—	83
Perovskite	2017	9.84	59	18.23	0.91	HTL	PAF	84
Perovskite	2017	14.07	69.91	20.88	0.97	HTL	—	85
Perovskite	2017	14.85	72.8	18.73	1.09	HTL	—	86
Perovskite	2018	10.17	65	16.33	0.95	HTL	COF(CON)	87
Perovskite	2018	19.07	78.3	23.6	1.031	AL (dopant)	COF	88
Perovskite	2019	6.36	54.33	15.38	0.76	HTL	COF	89
Perovskite	2020	14.28	73.38	19.98	0.97	ETL	—	90
Perovskite	2020	19.79	77.84	23.18	1.097	AL (dopant)	COF	91
Perovskite	2021	21.53	76.9	24.13	1.16	HTL	CMP	92
DSSC	2007	4.31	59	9.47	0.78	Electrolyte	—	93
DSSC	2008	6	51	11.86	0.72	Electrolyte	—	94
DSSC	2009	4.58	56	11.68	0.7	Electrolyte	—	95
DSSC	2009	8.35	68.4	16.26	0.751	Electrolyte	—	96
DSSC	2010	9.25	71	17	0.761	Counter electrodes	—	97
DSSC	2012	9.9	78	12.62	0.999	Counter electrodes	—	98
DSSC	2020	5.96	59	12.8	0.79	Electrolyte	—	99

reduced charge recombination.[92] POPs in OPVs, however, gradually shifts their role in the active layer to the HTL for better harnessing the energetic advantage and efficient charge transport to engineer the interlayer properties.[81] For DSSCs, the substitute of a liquid electrolyte prevents a short-circuit and demonstrates high durability.[94,99] Therefore, incorporating insights from chemistry, materials science, and physics, we aim to present a comprehensive retrospective to unravel the correlation between the intrinsic properties and the photophysical process. Through extensive charge dynamics analysis, a multifaceted process from photons to charges can be thoroughly understood.

2.1.1 Pores, backbones, and molecular properties. Porosity is one of the most unique and important features that define POPs. As shown in Fig. 2A, taking advantage of the lattice confinement and ordering, previous reports showcased the donor–acceptor heterojunction configuration through covalently anchoring fullerene to the pores *via* the click reaction.[100] The incorporation of C_{60} strengthens the system's absorbing capability in the visible wavelength region. Further time-resolved electron spin resonance (TR-ESR) shows an ultra-long charge carrier lifetime up to 2.37 ms.

Depending on the size of pores, it can further be divided into micropores (<2 nm), mesopores (2–50 nm), and macropores (>50 nm).[101] Since the domain size is pivotal for exciton diffusion and further polaron formation, common polymer frameworks employed for optoelectronic applications are prone to be microporous and mesoporous due to the exciton diffusion length.[102] However, smaller pore synthesis requires demanding synthetic controls to prevent pore collapse and skeleton interpenetration.[52,103] The versatility of pores also brings opportunities for dopants to be introduced into the open framework for enhanced conductivity, which is crucial for assisting fast charge transport.[49,104,105] Liu and co-workers[106] exploited the excellent electron-donating properties and the favorable stacking features to generate mixed-valence tetrathiafulvalene[107] complexes after iodine doping. The superior conductivity of 0.28 S cm^{-1} is three orders of magnitude higher than the value of the pristine sample (1.2×10^{-4} S cm^{-1}), which is among the highest conductivity reported. The improved performance can mainly be assigned to the proximity of tetrathiafulvalene units. However, in the same report, they also highlighted the concern on how to retain the record-high conductivity.

Since doping proves to be an effective strategy to fine-tune the conductivity, surface area, and morphology, its relevance with the energy level and interfacial properties remained elusive. Li *et al.*, therefore, adopted a computational approach to quantify the energetic shift concerning the Na dopant.[108] As depicted in Fig. 2B, the dopant position at the pore is calculated to be the least energetically favorable, rendering a large energy alignment mismatch between the COF and the graphene underneath. The preferential position of the dopant on the COF or in the COF/graphene complex proved to strongly hybridize between two moieties and reduce the charge injection barrier for favorable charge transfer. This work stressed the importance of dopant position pertaining to the interlayer properties, and the intriguing properties of dopant-induced work function shifting is relevant for charge extraction optimization.

Apart from traditional pre-designed building blocks to determine the pores, emerging post-synthetic modification methods render numerous pore surface engineering approaches to fine-tune the porosity. Kang *et al.* reported the successful incorporation of sulfonic acid to the pores by employing the biphenyl subunit. This post-synthetic sulfonation process drastically improves the conductivity to achieve a decent and long-term conductivity of 1.59×10^{-1} S cm^{-1}.[109]

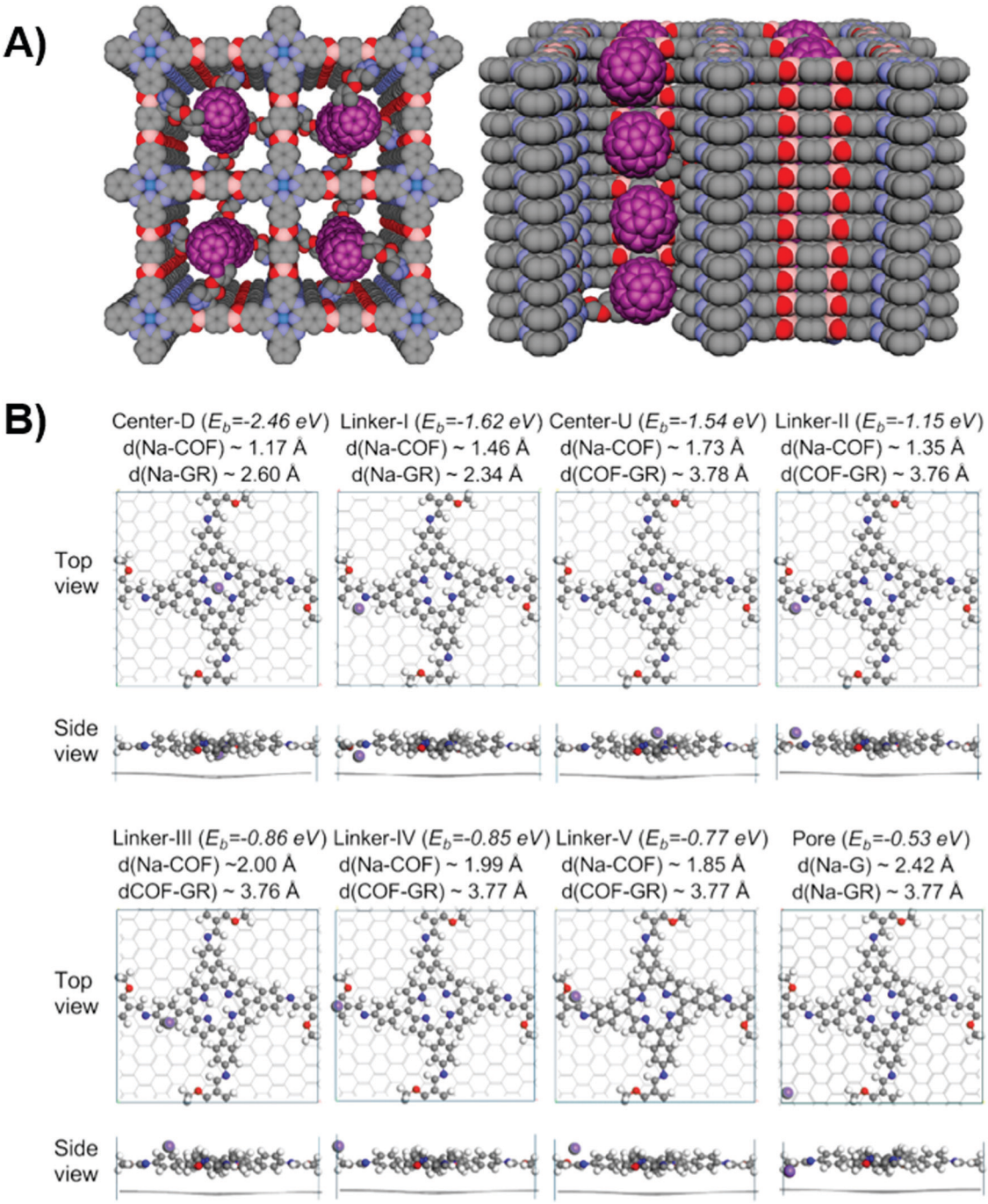

Fig. 2 (A) Top and side views of donor–acceptor COF with C_{60} (purple) integrated on the channel walls. Reproduced with permission from ref. 100. Copyright 2014, American Chemical Society. (B) Different Na dopants calculated preferential positions with reference to graphene substrate and COF. Purple, white, grey, blue, and red balls refer to Na, H, C, N, and O atoms respectively. Reproduced with permission from ref. 108. Copyright 2020, American Chemical Society.

Besides pore interface engineering, molecular orientation and morphological control are also of great importance for optoelectronic performance. Based on the aforementioned structural advantage over linear polymers, POPs should be promising candidates for an effective charge transport process. For OPV, the charge transport consists of intramolecular and intermolecular processes, where the former relies on the extent of π-conjugation and the latter depend on the interlayer van der Waals force.[110]

Strategies including side-chain engineering,[111,112] solvent interactions,[113,114] and temperature[115] have been widely explored to address the steric hindrance and ensuing molecular torsion and conformational property. Likewise, such approaches are also devised and implemented in the porous network.

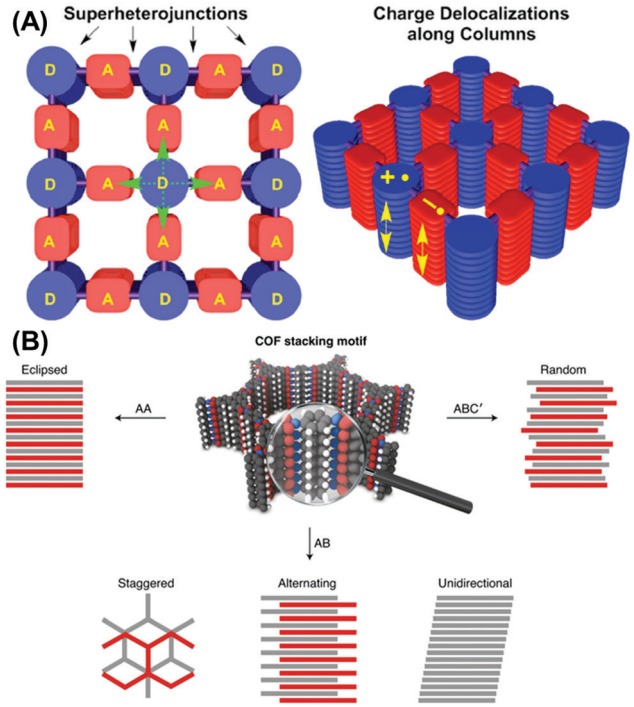

Fig. 3 (A) COF adopts donor–acceptor-like building blocks for building bi-continuous super-heterojunctions. Reproduced with permission from ref. 116. Copyright 2015, American Chemical Society. (B) Different stacking configuration for COF. Reproduced with permission from ref. 117. Copyright 2020, Springer Nature.

Judiciously choosing an electron-donating and withdrawing moiety, a bi-continuous donor–acceptor heterojunction can be synthesized.[105] In addition to complementary absorption benefiting from different moieties, the topology largely assists the charge migration process. As depicted in Fig. 3A, one donor is covalently linked with four adjacent acceptor units, which provides extra charge separation and transfer pathways. The spatially separate vertical π-column facilitates efficient charge transport of electrons and holes respectively while suppressing the charge recombination.

The unique molecular packing justifies the high mobility and long charge-separate state lifetime observed in those molecules. Since the π-column serves as a charge transport freeway, manipulating the molecular stacking is therefore of great relevance to achieve this performance. As shown in Fig. 3B, commonly stacking motifs can be categorized into AA, AB, and ABC′ stacking.[11,76] AA stacking promotes π-overlap between the layers and it is energetically more favorable compared to the other stacking modes.[118] For a photoactive layer in typical OPV, a planarized backbone configuration is preferred for face-on orientation for intermolecular charge transfer.[119] However, twisting and stretching of specific sub-units may cause the plane tilting and undesired packing mode. D_{CuPc}–A_{DI}–COFs, for instance, have a 20° twist angle caused by the H–H interaction of the PDI unit as well as the counter-tilt of the phenyl group.[116] To obtain fine packing behavior, Chen *et al.* investigated the fluorination effect on arene units for porphyrin–COF. The self-complementary π-electronic force proved to enhance π–π interaction, fine-tune the interlayer distance, and further reduce the bandgap, which translates to a high degree of crystallinity.[67] A few other topological-guided packing patterns are also reported by Bein and co-workers.[120,121] While weak intermolecular interaction hinders the charge hopping efficiency, strong co-facial packing could induce self-quenching and aggregation.[122] It is hence important to form a holistic understanding of the building block planarity, bond stretching and rotation, as well as the external environmental effect to control the interlayer property for successful PV integration.

Compared to crystalline COF, amorphous CMP does not possess well-ordered interlayer stacking, which shifts the synthetic attention towards engineering its own building blocks. Transferring the D–A backbone design strategy to CMP, the system can theoretically experience ultrafast charge transfer due to the push–pull effect of different units.[123] Mothika *et al.* demonstrated the bandgap engineering tactics through tuning the donor-to-acceptor ratio for F_xCMP synthesis, in which tetraphenylethylene (TPE) and 9-fluorenone (F) serve as the donor and the acceptor.[124] By increasing the acceptor concentration, the absorption is drastically red-shifted and the visible light-harvesting is also improved. This is assigned to energy transfer (ET) and intramolecular charge transfer. This enticing strategy along with solution processibility in common organic solvents may earn CMP its unique position in the PV area.

Ever since the advent of the 3D structure of POP,[68] the attention for high dimensionality doesn't seem to halt. Owing to its unique topological and geometric advantage, charges and other species can migrate through more pathways rendered by the accessible framework to promote charge transport.[125] Various types of pore sizes, shapes, and configurations endow endless opportunities for emerging applications.[126–128] However, it inevitably raises the question of whether the excitement is conducive and can be transferrable for PVs. Firstly, when accessing the topological evolvement, more versatile 3D structures would require bond twisting and specific tilted angles, especially at the vertices, to maintain the rigid and periodic structure in different dimensions. Hence, the ensuing disturbance of π-conjugation is inevitable and hampers the charge delocalization.[129] Since the 3D porous framework prevails over its 2D counterparts concerning the outstanding interpenetration and porosity, which makes it futile to strive for incorporating highly π-conjugated backbones. Thus, it leaves further adjustability of bandgap and conductivity to doping. Nevertheless, Byan *et al.* successfully realized fully sp^2-hybridized 3D p-POP.[34] The aromatization is achieved *via* Diels–Alder cycloaddition followed by acid-promoted cyclodeoxygenation. Instead of utilizing 3D POP as the sole photoactive component, researchers also explored the effect of its corporation with perovskite material, which showed enhanced crystallinity and excellent charge mobility due to the close contact and energetic benefits between those two materials.[88] Hence, exploiting the structural advantage to assist the photophysical process is highly promising to enhance device performance. To effectively control the topology, properly addressing steric hindrance is of top priority. Some approaches decorated

the building blocks with methoxy and methyl groups to achieve a non-interpenetrated topology,[103] others substitute methoxy with phenyl groups to realize highly-crystalline unprecedented structures.[130] It is worth mentioning that much effort is paid to increase the rigidity and porosity after guest removal, and it should not be a major concern for PV applications since the active component compositions and locations are permanently decided once the synthesis is completed. In the meantime, the effort to drastically increase the void inside the framework is not preferred for the sake of effective charge dissociation processes. However, similar to the consideration of pores, an overly dense topology with ensuing ultra-small pores will inevitably experience high electrostatic interaction, which may lead to polaron trapping and reduced charge mobility.[49] Therefore, with judicious design and selection of promising building blocks and post-synthetic modification tools, a functionality-driven synthesis that fully reveals the structural potentials could propel the further implementation of 3D POPs in solar cells.

The surface area is immensely stressed when deploying POP as a functional material. Unlike previously mentioned properties, the extensive discussion of its relevance with the photophysical process has yet been presented and is far from conclusive. To date, a large surface area bestows excellent interfaces for chemical reactions and sensing unit anchors, as well as high capacitance for retaining the charges, which render the feature conducive for catalytic processes, gas adsorption and sensing, as well as supercapacitors.[131–134] Unfortunately, these properties are not directly transferrable for PVs. Considering the host–guest configuration, the surface area in this scenario represents the donor–acceptor interface, which governs the charge dissociation processes. While the domain sizes determine the ultimate number of excitons that diffuse to the interface, the interface property directly impacts the success of charge separation. The charge transfer (CT) state, formed at the interfaces, provides an energetic impetus for splitting excitons.[135] Since the CT state is an intermolecular state, whose emission yield is significantly lower than the local exciton (LE) state, it contributes to the voltage-losses through non-radiative pathways.[136,137] In bulk heterojunction OSCs, several studies pointed out the potential strategy to reduce the CT state density by reducing the donor-to-acceptor ratio, which equivalently shrinks the interfacial area.[138,139] Given the versatile design of the skeleton-pore introduced in the above sections, POPs could also benefit from the same approach by tailoring the surface area as well as pore sizes to obtain a precise interfacial profile. Other promising techniques such as oscillator-strength borrowing through LE-CT hybridization[137] and employing ternary components[140] are also worth exploring. Noticeably, recent studies proved the relevance of quadruple moments and interfacial energy levels, which further stresses the imperative of fine-tuning the electrostatic interactions and molecular orientation at the interfaces.[141–143] Those concerns can potentially be addressed by the post-synthetic modification and steric hindrance engineering mentioned previously.

2.1.2 Photophysical process for POP. Based on the photoactive configurations, common POPs suitable for optoelectronics can be clustered to either host–guest or D–A super-heterojunctions (without guest molecules). While the former shares vast similarities with conventional organic solar cells, the latter remains elusive regarding its photophysical process. As mentioned above, due to poor film quality and/or polycrystal aggregates, the optical characterization of POP faces huge obstacles to feature fine nanostructures. They either scatter light or the signal-to-noise ratio is relatively low to discriminate any discernible feature for effective electronic and charge dynamics investigations.[144–146] To date, most photophysical studies heavily focus on COFs, which is predominantly attributed to its better π–electronic structure, film formation, and burgeoning facile synthesis techniques. As a COF photoactive layer was successfully incorporated for energy-conversion devices, the research group of Jiang extensively explored the charge-separated state features.[100,116,147] Through TR-ESR, they observed the ultra-long charge carrier lifetime up to milliseconds for the AA-stacked bi-continuous super-heterojunction COF. The thrilling results then lead to further studies which reveal ordered COF's high electron and hole mobility through π-column,[118] and those efforts can potentially contribute to optimizing the charge extraction for device-level integration. However, as depicted in Scheme 1, the complete process of photons to electrons necessitates an in-depth understanding of absorption, diffusion, separation, as well as transport and extraction. Therefore, commensurate attention should also be paid to the process that precedes charge separation.

For the case of POPs, it is generally recognized that exciton-exciton annihilation (EEA) is the underlying mechanism for charge dissociation. Unlike the host–guest system, where the intermolecular energy-level difference provides the driving force to separate the excitons, excitons formed in D–A super-heterojunction COFs reside in the same molecular domain, the EEA therein hence facilitates the dissociation by overcoming the binding energy. Jakowetz *et al.* first demonstrated a systemic characterization of the excited state dynamics of COFs.[148] They primarily adopted photothermal deflection spectroscopy instead of conventional UV-Vis spectroscopy, which can greatly circumvent the interference from the light scattering and garner more sub-bandgap features. In the charge decay measurement assisted by time-correlated single-photon counting (TCSPC), they observed similar decay kinetics for TT and BDT bridging units, comprising nanoseconds of slow decay components after initial decay. Under short-time transient absorption (TAS), the fast quenching of stimulated emission (SE) without significant correlation with photoinduced absorption (PIA) strongly indicates the occurrence of EEA. They also detected negative features for thicker films, whose decay kinetics suggest that EEA does not merely lead to recombination to the ground state. Extending the probe to a long-time scale, they assign the ultra-long lifetime to trap-assisted recombination. Eventually, they summarize the overall photophysical process, which is depicted in Fig. 4; the initially generated excitons undergo EEA and are "trapped" in different moieties and spatially impedes charge recombination. They also point out the possibility of EEA occuring between sheets, which could lead to more research on the relevance of structural as well as interfacial behavior with EEA.

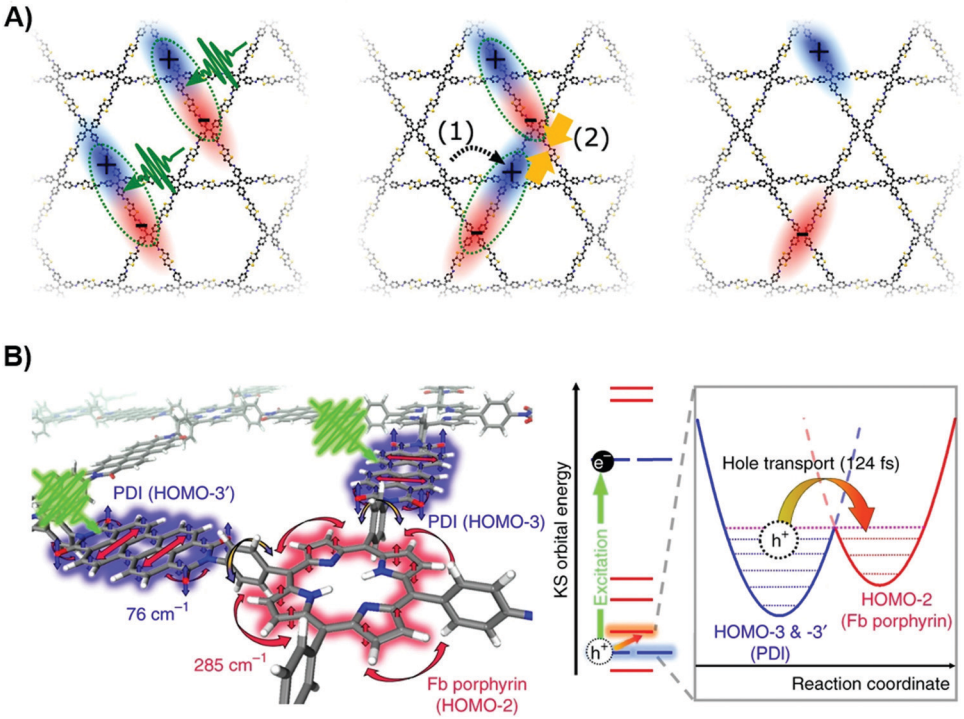

Fig. 4 (A) Photophysical processes of simple 2D COF, excitons are formed after photoexcitation, and they then experience EEA and are "trapped" in different moieties for charge transport. Reproduced with permission from ref. 148. Copyright 2019, American Chemical Society. (B) Schematics for hole transfer kinetics with the torsional motion of benzene rings for PDI-porphyrin COFs. Reproduced with permission from ref. 149. Copyright 2019, Springer Nature.

Regarding the time scale to effectively dissociate the excitons, Jin *et al.* characterize the charge dynamics of D_{ZnPc}–A_{NDI}–COF with TAS.[147] By obtaining the time scale of radical formation at a selective wavelength, they estimate the rate of charge dissociation to be 5.5×10^{11} s^{-1}. Ultra-fast electron transfer and dissociation is observed for both benzonitrile and DMF solvent. Despite the fact that COF in DMF exhibits improved solubility and absorption due to delamination, its thinner and fewer layers feature shortened the charge carrier lifetime. Therefore, the film thickness and layer structure are crucial for long-distance charge delocalization and retaining the charge carrier lifetime.

To further elucidate the dynamics of photogenerated charges, Kim *et al.* combine both TAS and theoretical simulation to unravel the charge transfer kinetics between different moieties.[149] Three electronic states were identified through species-associated difference spectra in TAS global kinetic analysis. By comparing TAS spectra of PDI-porphyrin COFs and free-base porphyrin, along with non-adiabatic molecular dynamics simulation, the first to second transition is assigned to ultra-fast hole transfer from the PDI unit to porphyrin moiety. The researchers argued that the quasi-degeneracy of molecular orbitals in both vertical and horizontal directions contributes to the hole dynamics. Further simulations confirm the second transition is necessarily the relaxation process of the excited states, which mainly manifests interlayer charge transport. From the distinct features of 76 cm^{-1} and 285 cm^{-1} vibrational modes (shown in Fig. 4B), it is found that the torsional motion of the benzene ring serves as a π-bridge to facilitate intramolecular charge transfer. Therefore, the overall photophysical profile can be concluded as a lattice phonon-assisted charge transfer process.

In light of the specific process of exciton diffusion, it bears a significant role in retaining the photogenerated carriers before any dissociation process. Flanders *et al.* recently examined COF-5 with extensive transient absorption techniques to unravel the exciton transport.[102] Noticeably, the intramolecular charge transfer state, which is necessarily an excimer state, is significantly more emissive than the CT state in a conventional bulk-heterojunction organic mixture. By characterizing COF with different domain sizes, they discovered that the larger domain size favors the co-facial orientation, and the conjugation is enhanced due to improved rigidity. These contribute to the better formation of excimers. As depicted in Fig. 5A, three distinct processes are identified. 4ps is the excimer formation lifetime, whereas 160 ps corresponds to the time for excimer relaxation. It then further undergoes long-lived decay kinetics. By extracting the decay component under high fluence, the researcher calculated the diffusion coefficient to be 0.09 cm2 s^{-1} and the diffusion length to be around 5 nm. The short diffusion length is assigned to the short-lived exciton lifetime. Since EEA is proportional to excited state density, the researchers explore the size-dependent analysis of EEA by varying fluence. The results show a much more prominent EEA impact on decay kinetics for smaller crystallites. The researchers ascribe this phenomenon to higher diffusional freedom and less surface trap-assisted EEA in

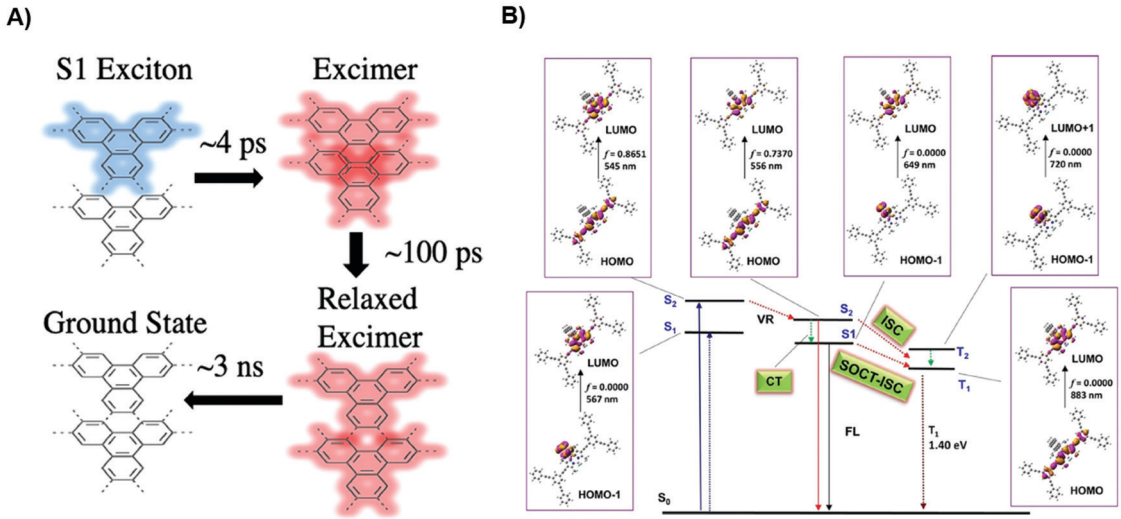

Fig. 5 (A) Excited-state dynamics for COF-5 with a lifetime of each electronic state. Reproduced with permission from ref. 102 Copyright 2020, American Chemical Society. (B) Excited states dynamics for CMP-1 with the decoration of PAH upon photoexcitation. VR, FL, and SOCT stand for vibrational relaxation, fluorescence, and spin–orbit charge transfer respectively. Reproduced with permission from ref. 152. Copyright 2021, John Wiley & Sons.

larger domains. This work highlights the importance of domain size-dependent diffusion dynamics and the necessity to prolong the exciton lifetime.

Given that strenuous effort is paid to characterize COF through various optical methods to achieve reliable and distinguishable features, it is no surprise that the investigation of amorphous POP excitonic states is even more scarce. Rao *et al.* recently revealed the light-harvesting capability of two dynamic CMPs, namely Py-PP and Py-BPP.[150] By exploiting the guest-induced swelling to load hydrophobic luminescent chromophores, a tunable solid-state emission can be achieved. The energy transfer between the host material and the guest dye is confirmed through the photoluminescence spectral feature obtained at each emission wavelength. The shortened lifetime of the host framework upon encapsulation of the DMDP dye further confirms the occurrence of ET for fluorescence quenching. Since a good absorber is also a good emitter,[151] this strategy for effectively tuning the emission profile can also be transferrable for highly efficient donor–acceptor PVs.

By decorating the backbone with polycyclic aromatic hydrocarbons (PAH), Peng *et al.* studied the energy and charge transfer of a heavy-metal-free CMP system.[152] It is shown that the intersystem crossing (ISC) and charge separation can be promoted through fine-tuning the aromaticity of the CMP. The long-lived triplet state is favorable for interfacial energy transfer, which is corroborated by TAS results. The small charge transfer resistance upon PAH incorporation, observed from electrochemical impedance spectroscopy, further promotes the charge dissociation to achieve higher photocurrent. Further simulation suggests a higher oscillator strength for BODIPY moiety upon photoexcitation, corresponding to the S_0 to S_2 transition (Fig. 5B). After vibrational relaxation, the localized Bodipy singlet state is populated, which proves the photo-induced intramolecular charge transfer. Density-functional theory (DFT) calculation indicates an additional ISC pathway is created after PAH decoration, which is necessary for the transition from S_2 to S_1, then T_1. Even though this study intends to implement the strategy for efficient photocatalysis and ISC is not favorable for PV applications, the insights from different excited states can further facilitate the voltage loss studies through triplet states as well as charge dynamics changes upon backbone decoration. Furthermore, this kind of CMP system may be a suitable candidate for triplet–triplet annihilation photon-upconversion,[153] which provides an alternative strategy for solar energy conversion.

Taking advantage of both the charge dynamics and energetics, POP provides synergistic enhancement to device photovoltaic performance. Despite its infancy in POP, Yao *et al.*[154] synthesized a porphyrin-based 2D-COF TPA@TAPP that presents both energy transfer and charge transfer (Fig. S3, ESI†). Clear and significant quenching as well as rapid kinetic decay are observed and derived from TRPL and transient absorption spectroscopy, respectively. The dual effect enabled by CT and ET renders 1.8 times higher photocurrent generation along with sharp rise and fall edges during transient photocurrent measurements. Those results indicate better charge separation and reduced charge recombination, which further supports the exploitation and engineering of charge dynamics and energetic profile to improve 2D-COF photophysical properties.

2.2 POP-based organic solar cells (OPV)

In the past five years, the incorporation of POPs in the OPV photoactive layer has not seen concomitant progress as compared to other applications. Research efforts have gradually shifted from solely utilizing POPs as the photoactive component to the charge transport layer. The only promising report on the active layer was presented by Xu *et al.*, in which they simulated that the expected PCE of quinazoline-based COF/ZnSe heterojunctions could potentially reach 22.32%.[155] To fully take advantage of the direct bandgap and near-infrared

(NIR) absorption of Q-COF, the ZnSe monolayer is chosen as the acceptor to form type-II offset (Fig. 6A).

Upon consideration of lattice strain, the PCE can be further improved. The low cleavage energy and higher mass-energy density render Q-COFs a strong candidate as a donor material. However, since the report is entirely computational, it fails to take into consideration the film formation, morphology, molecular orientation, and charge extraction aspects. Another intriguing progress by Bildirir *et al.*[32] showcased the PV application of an n-type solution-processable conjugated polymer network (PNT1). Synthesized through Stille cross-coupling reaction, PNT1 obtains high thermal stability and adequate photon absorption in the visible light spectrum. Using PNT1 as the acceptor component in the bulk, the device adopts an inverted configuration of ITO/ZnO/PTB7-Th:PNT1/MoO_3/Ag, which exhibits a PCE of 1.18% and an EQE of 25%. The authors argued that the low FF can either be caused by low charge carrier mobility or the high miscibility of the donor and acceptor material. Zhang *et al.*[80] adopted a hyper-branched HP-PDI to pair with PTB7-Th. The hyper-branched structure and the abundance of terminal PDI units fine-tune the domain size and balance the hole/electron mobility. The resultant device achieved a PCE of 2.15% and it remarkably retained 91% of its original efficiency after 6 days (Fig. S1, ESI†), showcasing superior stability enabled by structural advantages. On the other hand, Fu *et al.*[82] proposed the employment of a soluble POP as a donor material. PDPP-C20, which obtains long branched alkyl chain, demonstrates great solubility in common solvents and presents decent hole mobility. Paired with IT-4F, a remarkable value of V_{oc} = 0.8 V is achieved. However, the unsatisfying FF lags the PCE to merely 2.46%. Despite the low PCE, the device steadily operates up to 650 hours under ambient conditions while reserving 90% of the J_{sc}, V_{oc}, and PCE (Fig. S2, ESI†), demonstrating phenomenal stability to external species. The concept of a solution-processable conjugated polymer network brings excitement to manufacturing and other promising optoelectronic applications. Moreover, numerous insights from commonly investigated organic blends are therefore transferrable to fine-tune the nanomorphology and interfacial properties *via* diverse microfabrication techniques.[156–159]

Concerning the emerging application as the charge transporting layer, Yang *et al.* electrochemically deposited CMP films onto the substrate, which serves as the HTL for OPVs.[64] The thickness of the film is controllable through the scan cycle, providing facile engineering techniques to improve the charge transport. The work function (WF) of the electropolymerized CMP is around 5.03 eV, which forms an energy cascade for effective charge transport. (Fig. 6B) It outperforms PEDOT:PSS since it obtains higher WF for better hole extraction. By sandwiching PTB7-Th:$PC_{71}BM$ between CMP (HTL) and PFN (ETL), with electrode options of ITO and aluminum, the device

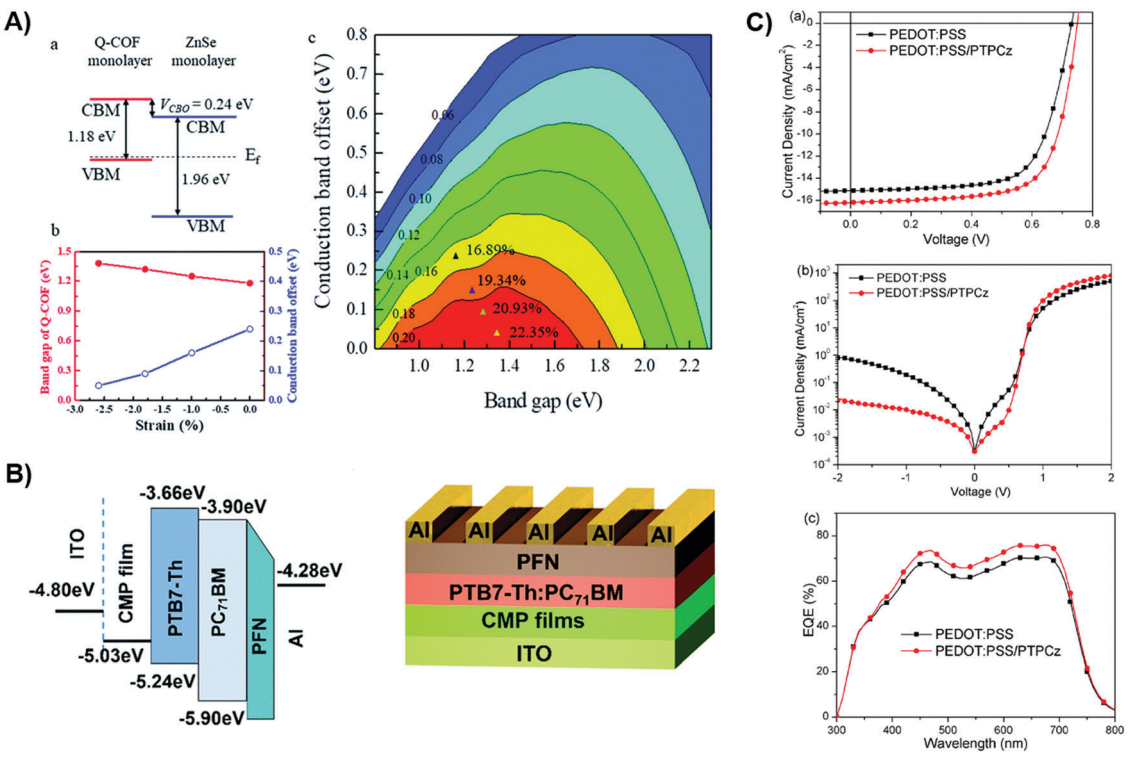

Fig. 6 (A) Calculated bandgap and energy alignment for Q-COF and ZnSe; the lower figure is the energy level with relevance to the lattice strain, along with simulated PCE mapping with reference to the Q-COF bandgap and conduction band offset. The colored area represents increasing strain. Reproduced with permission from ref. 155. Copyright 2020, Royal Society of Chemistry. (B) Device configuration and energy levels of CMP incorporated OPV. Reproduced with permission from ref. 64. Copyright 2018, Royal Society of Chemistry. (C) *J*–*V* characteristics under light and dark, as well as EQE spectrum under 1 sun condition. Reproduced with permission from ref. 81. Copyright 2017, Elsevier.

shows an open-circuit voltage (V_{oc}) of 0.8 V and short-circuit current (J_{sc}) of 16.14 mA cm^{-2}, which are both higher than the case of PEDOT:PSS. The authors ascribe the V_{oc} increase to the higher built-in potential and suppressed bimolecular recombination, whereas the J_{sc} improvement stems from the higher EQE.

Instead of fully replacing the original HTL, Liu *et al.* modified the PEDOT:PSS HTL by inserting a POP film, which is an interlocked network comprising carbazolyl triphenylethylene derivative (TPCz) building blocks, namely PTPCz.[81] The permanent porosity of the POP films can form close contact with electrodes and the photoactive layer to assist charge transport. The resultant device exhibited a high PCE of 8.54%, a V_{oc} of 0.74 V, a J_{sc} of 16.23 mA cm^{-2}, and a FF of 0.71. As illustrated in Fig. 6C, the reduced dark current level signifies blocked leakage pathways and higher shunt resistance, which contributes to V_{oc} enhancement. The contact resistance is minimized due to the structural pores of the POP films. Hence, smaller series resistance combined with a higher work function benefits the hole transportation, leading to a high FF.

A few years after the first incorporation of a CMP HTL in an OPV, Li *et al.* revealed more insights into this interfacial strategy *via* various optoelectronic characterization techniques.[65] They stated that the substitution of carbazole groups facilitates the molecular planarity to help extend electron delocalization, which paves the way for efficient charge transport. The CMP-modified PEDOT:PSS turns out to effectively deepen the HOMO level of the latter, and it exhibits great transmittance. Through V_{oc}–light intensity measurement, the results show that the CMP-modified samples suffer less from trap-assisted recombination. From J_{sc}–light intensity analysis, it is observed that the bimolecular recombination profile remains unchanged. The decay kinetics obtained from transient photovoltage indicates that the incorporation of CMP prolongs the charge carrier lifetime and expedites the charge extraction process. Those critical charge dynamic insights further support the promising strategy to adopt CMP-modified PEDOT:PSS as the HTL.

Besides the enhancement in charge transport layers, the incorporation in the electrode has also been recently demonstrated a promising approach to replace commonly used metals. Yu *et al.*[160] showcased a highly reflective nanoporous polymer incorporated back electrode with thickness-dependent opacity and transmission. Through CO_2 diffusion, the nanofoamed PMMA presents an excellent reflectance profile compared to the silver electrode in the Vis-NIR region. J_{sc} is slightly compromised due to the energy level mismatch associated with the thickness of the rear polymer electrode layer. Nevertheless, the overall solar cells retain the original photovoltaic performance and achieved 6% of average visible transmittance (AVT) with less than 5% loss of PCE. This report highlighted an effective strategy to optically engineer the electrode *via* porous polymers. However, more specific porosity-related multi-scattering and diffuse reflection models and photophysical processes required further investigation to fine-tune the energy landscape and optical properties.

2.3 POP-based perovskite solar cells (PSCs)

Classic perovskites are unique structural materials that adopt the chemical formula of ABX_3.[161,162] More specifically, the most studied and promising types are organic–inorganic lead halides, namely $MAPbI_3$ and $FAPbI_3$, in which MA and FA stand for methylammonium and formamidinium, respetively.[163–165] Recent years have seen rapid growth of PSC research. Strategies including topological design, material combination, microfabrication techniques, and device physics have been heavily explored.[166,167] The unique porosity and tunable electronic structure of POP materials could potentially contribute to the device performance enhancement. As opposed to the trend observed in OPVs, the presence of POPs in both the photoactive layer and HTL/ETL components has been reported, which opens a new pathway to further boost the perovskite performance.

3D POP boasts of its superior geometric features, which provide more accessible pathways for charge dynamics and photoelectric activities. Wu *et al.* reported a spirobifluorene-based SP-3D-COF doped PSC with significantly improved PCE up to 19% compared to undoped samples.[88] Exploiting the multidimensional charge transport of the SP-3D-COF, the device with the inverted p–i–n configuration (Fig. 7A) showed low dark current density and good diode rectification. All key parameters regarding J_{sc}, V_{oc}, and FF are greatly boosted. Upon bulk doping, the absorption is red-shifted due to the extended conjugation. The researchers further rationalize the simultaneous gain in device performance through DFT calculations. Simulations suggest the formation of a low-lying symmetry-breaking CT state that assists the free flow of excited electrons through a spirobifluorene moiety. Meanwhile, the HOMOs and LUMOs preferably localize at the far end of each molecule, and this spatial preference effectively suppresses the charge recombination. The larger area of the biphenyl-group in the case of SP-3D-COF 2 improves the interfacial contact with $CH_3NH_3PbI_3$, thus explaining the better morphology profile. Additionally, it also leads to more available HOMOs to accept the excited electrons from perovskites, which promotes charge generation.

To further elucidate the interfacial properties between POP and perovskites, a systematic study was conducted by Mohamed *et al.* on 2D imine-linked Car-ETTA and TFPPy-ETTA COFs.[91] By incorporating a porous scaffold, a blue-shifted PL peak is detected, indicating defect passivation for COF-modified ETTA HTL. This further leads to enhanced crystallinity of the perovskite through additional nucleation sites. The device with the configuration of (ITO)/PTAA/COFs/$(FAPbI_3)_{0.83}(MAPbBr_3)_{0.17}$-$(CsPbI_3)_{0.05}$/PCBM/BCP/Ag, exhibits a high PCE of 19.79% under the forward scan. Significant faster decay kinetics revealed by TCSPC suggests excellent hole transfer characteristics for both TFPPy-ETTA and Car-ETTA COFs. By investigating the photocurrent density trend with effective voltage, authors are convinced that higher exciton generations and better charge collection directly translate to a higher J_{sc} level. This work highlighted the structural impact of COF on its resultant device performance.

The competent hole-transporting capability along with deep energy alignment of different POPs have already demonstrated their compatibility as HTLs. Effort has also been dedicated to

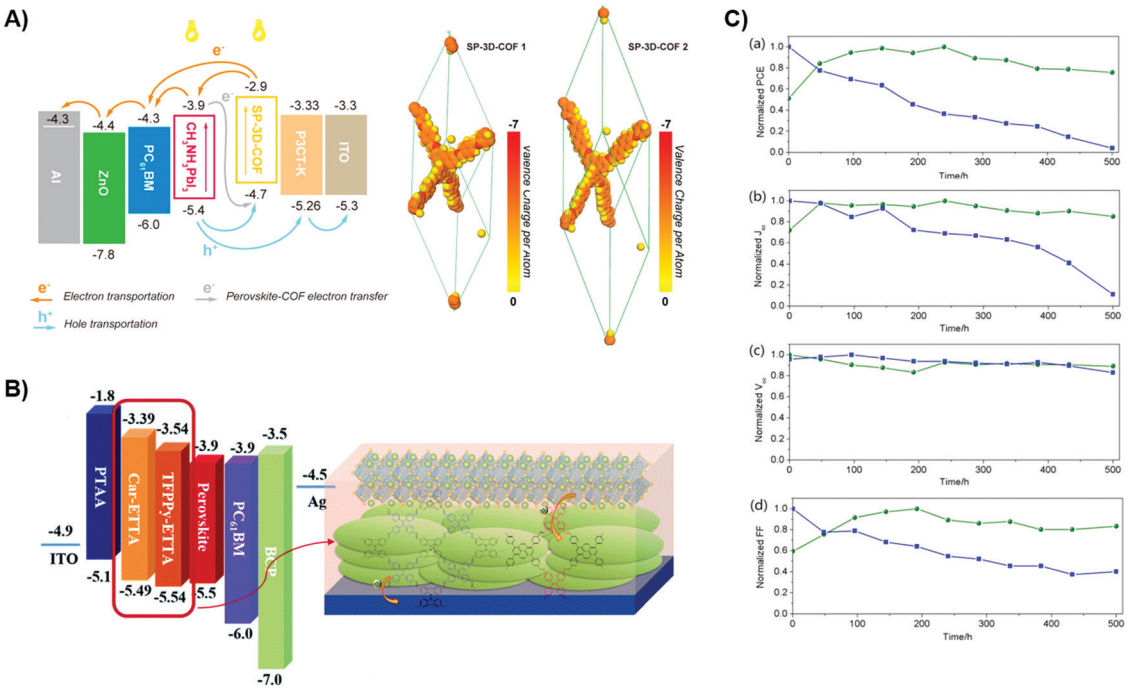

Fig. 7 (A) Device configuration of SP-3D-COF doped PSCs with holes and electrons flow upon photoexcitation. Reproduced with permission from ref. 88 Copyright 2018, American Chemical Society. (B) Device configuration and COF stacking behavior for Car-ETTA and TFPPy-ETTA COFs. Reproduced with permission from ref. 91. Copyright 2020, Royal Society of Chemistry. (C) Key PV parameters stability experiments. Figures from top to bottom are PCE, J_{sc}, V_{oc}, and FF respectively. Reproduced with permission from ref. 84. Copyright 2017, American Chemical Society.

employing POP in PSCs to circumvent the acidity problem of PEDOT:PSS. Through electropolymerization, a PAF-86 film was deposited onto ITO substrate as the HTL by Wang *et al.*[84] Space charge limited current (SCLC) results show moderate hole mobility in PAF-86 HTL. Interestingly, the fabricated device performance is enhanced without any encapsulation. The authors ascribe such improvement to the better surface contact between PAF-86 and the perovskite. Later they performed a stability test on the device (Fig. 7C), the retained PCE over 500 hours marks the suitability of utilizing PAF-86 as long-term stable PSC components. This effect is assigned to the hydrophobicity of the porous film that greatly slows down the humidity-related degradation process.

Apart from a structural strategy, a new approach adopting thin-film material as the HTL has also been explored. Park *et al.* reported a solvent treatable covalent organic nanosheet (CON),[87] which is incorporated into PSC for effective hole extraction. Atomic force microscopy results indicate the film quality of PEDOT:PSS is highly dependent on the roughness of the CON underneath. The roughness, on the other hand, can also translate to a larger surface contact area, which assists charge transfer. The strong PL quenching corroborates this argument. Owing to the remarkable electron blocking function and hole-transporting capability of CON, the resultant device employing CON-10 boosts the PCE to 10.7%. Since CON's morphology is solvent-dependent, it provides a facile engineering method to fine-tune the interlayer property.

The rigorous processing condition of POP due to its rigidity strongly inhibits its implementation in a modern solar cell. To tackle such challenges, solubilizing groups have been introduced into the backbone.[168] Lim *et al.* recently utilized a solution-processable T-POP as a secondary electron transporting layer (Fig. 8B), exhibiting a 13% of PCE increase.[90] The contact angle experiment proves that T-POP presents hydrophobicity towards ambient species, whereas its hydrophilic carbonyl and amide groups improve the morphology. The authors partly ascribe the J_{sc} increase to augmented perovskite crystallinity benefiting from T-POP. The high electron mobility and π–π stacking of T-POP further promote the charge transport and extraction. Very recently, Fu *et al.*[82] synthesized a COF-like 2D POP (PDPP-C20) *via* side-chain engineering to incorporate DPP derivative. By constructing a D–A type polymer and weakening intermolecular interactions, the dual role of charge extraction and passivation is reinforced, achieving an ultrahigh PCE of 21.92%. A clear spectroscopic feature gained in FTIR justifies the passivation effect, which suggests the interaction between C═O and under-coordinated Pb^{2+} defects. Besides synergistic improvement in photovoltaic parameters, the reduced hysteresis is also observed, suggesting promising suppression of ion migration in perovskites is potentially attainable through the incorporation of POP.

In addition to the abovementioned reports, Fu *et al.* employed a dopant-free 2DP-TDB to achieve a champion PSC efficiency of 22.17%.[92] By introducing bulky alkyl chains to the polymer, the solubility is drastically improved. The excellent crystallinity and strong face-on orientation (Fig. 8C) revealed by Grazing Incidence Wide-Angle X-ray Diffraction (GIWAXS), justifies its high hole mobility and great charge transport capability.

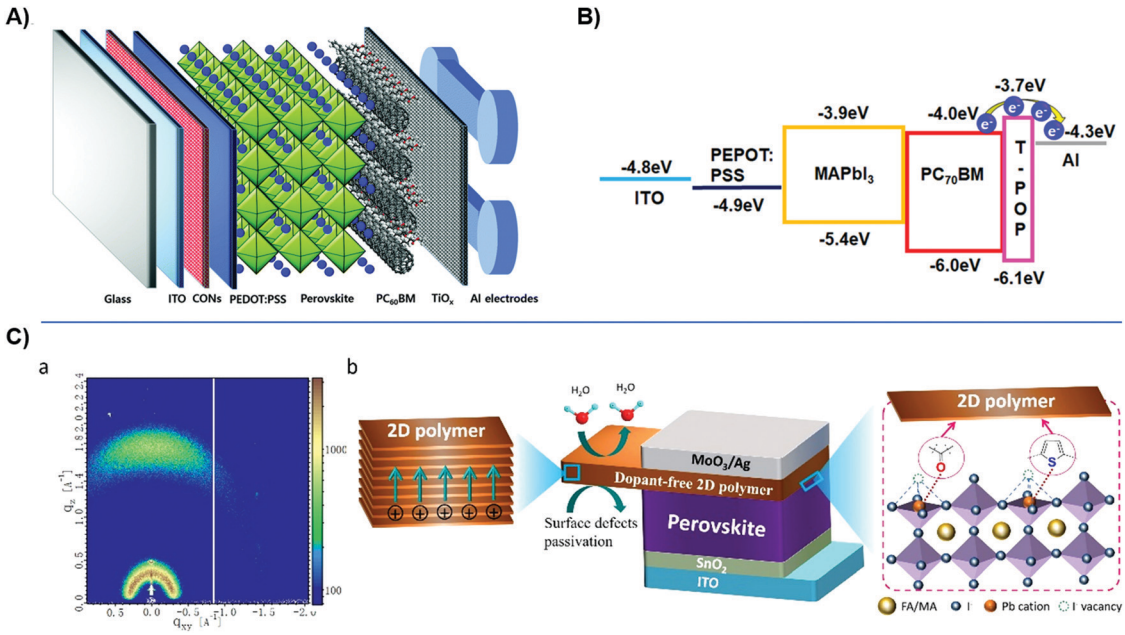

Fig. 8 (A) Device configuration of CON/PEDOT:PSS HTL incorporated PSC. Reproduced with permission from ref. 87. Copyright 2018, Royal Society of Chemistry. (B) Device incorporating T-POP as a secondary ETL. Reproduced with permission from ref. 90. Copyright 2020, Elsevier. (C) GIWAXS plot with device configuration. Reproduced with permission from ref. 92. Copyright 2021, American Chemical Society.

X-ray photoelectron spectroscopy (XPS) further shows the interaction of thiophene units of 2DP-TDB and undercoordinated Pb^{2+} in perovskite, which effectively passivates the surface defect by Lewis bases to prevent trap-assisted recombination and promote charge transport. The synergistic effect of adopting 2DP-TDP along with its deep HOMO level makes it a competitive substitute for commonly used doped spiro-OMeTAD.

2.4 POP-based dye-sensitized solar cell (DSSC)

First invented in 1988,[169] dye-sensitized solar cells have earned their unique place in PVs due to their lightweight, low cost, semi-transparent, and flexible properties.[170–172] The superb PCE maintenance under low light intensity marks its presence in various indoor applications.[173] Upon photoexcitation, the electrons from the photosensitized dye reach their excited state. Then, those excited electrons are injected into the conduction band of the adjacent semiconductor, typically TiO_2. Subsequently, they flow towards the contacts and are eventually collected by the counter-electrode through the external circuit.[174] The loss of electrons is compensated through redox activities in the electrolyte, which commonly involves the iodide and triiodide. Triiodide subsequently diffuses toward the counter-electrode for further reduction, which forms the redox cycle. The common challenges DSSC faces are the removal of heavy metals, corrosion and long-term stability of liquid electrolyte, dye adsorption, and energy alignment.[175] POP, owing to its intrinsic porosity, tunable features, as well as moderate conductivity, can be exploited as a competent material substitute as device components.

The highly porous structure along with a large surface area provides more redox sites and ionic loading capability to achieve higher ionic conductivity as well as better interfacial property with the electrode.[176] Thomas *et al.* recently synthesized and implemented a porous membrane (PMMA/PIL/PIN) based quasi-solid state (QSS) electrolyte in DSSC.[99] As exhibited in Fig. 9A, upon the incorporation of PIL to the PMMA membrane, the pore largely shrinks due to phase inversion. The end product of PMMA/PIL/PIN from the SEM image shows an increased number of pores and pore volume. Benefiting from the superior thermal stability of PIN, the porous membrane demonstrates great potential as opposed to the thermally susceptible liquid electrolyte. It is further explored that the high porosity and great interconnectivity lead to a high uptake of electrolyte, which contributes to ionic conductivity enhancement and large diffusion constant of redox species. The high V_{oc} observed in the assembled device is ascribed to the charge recombination suppression. The uniform surface coverage and intimate contact over TiO_2, and the imidazolium content of PIL, successfully passivate the interfacial defects. Moreover, the migration of electron-deficient Li^+ towards the interface is significantly circumvented due to chelation with PMMA, which helps suppress the recombination. The viscosity that impedes its penetration into TiO_2 compromises its J_{sc}. Nevertheless, the device retained 85% of its initial performance after 250 hours, indicating its great long-term stability over liquid electrolyte.

As mentioned above, the replacement of Pt electrodes is one of the heaviest researched topics. Effort has been made to incorporate microporous polyaniline (PANI). However, its instability remains undesirable for long-term efficient devices.[177] Ahmad *et al.* integrated a nanoporous poly(3,4-propylenedioxythiophene)(PProDOT) layer into DSSC, showing a maximum PCE over 9%.[97] As expected, the enormous surface area and porosity translates to higher catalytic activity and lower charge-transfer resistance. The only inferior performance of PProDOT incorporation is the reduction

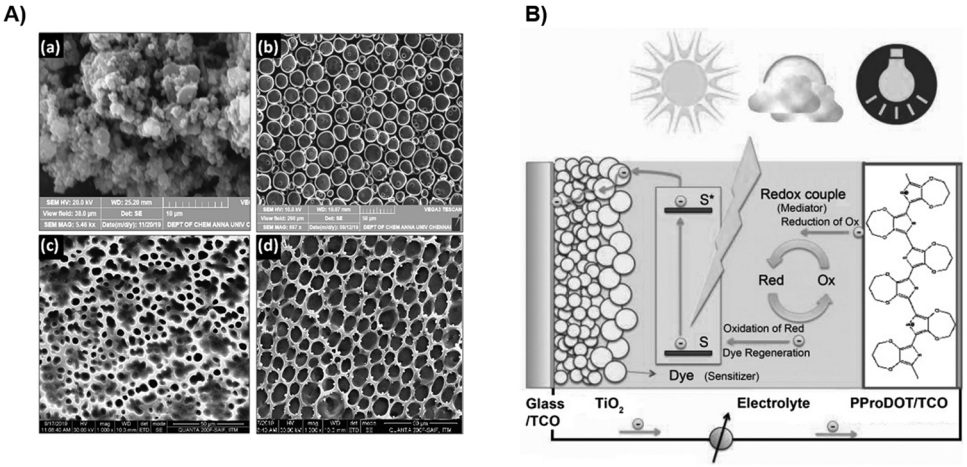

Fig. 9 (A) SEM image for PIN, PMMA, PIL/PMMA, and PMMA/PIN/PIL. Reproduced with permission from ref. 99. Copyright 2020, Elsevier. (B) Device configuration with the PProDOT electrode. Reproduced with permission from ref. 97. Copyright 2010, John Wiley & Sons.

of V_{oc}, which is assigned to the impurity during synthesis. To further explore the PProDOT cathode potential, the same group introduces dialkyl groups as side chains attached to the backbone, which induces improved solubility.[98] Despite the low FF due to reduced conductivity, it still outperforms the Pt electrode with high J_{sc} and PCE values. They argue that bulky groups may hinder the mass diffusion process.

3 Outlook and perspective

Despite its strong light-harvesting capability with strong electron-donating/withdrawing features, employing POP as the sole photoactive component faces severe challenges to rival other photoactive materials. The insoluble nature and low crystallinity gradually shifted the research effort towards its unique structural advantage to improve charge transport and interfacial properties. The POP-modified HTL demonstrates strong compatibility in PSCs with over 20% efficiency. Recent years have also witnessed the progress of unveiling the excited state dynamics of POPs and possible POP-modified electrode/electrolyte applications for DSSC.

The donor–acceptor super-heterojunction design in COF and other POPs largely promotes electron delocalization, induces ultrafast photoinduced charge transfer, and red-shifts the absorption spectra. At optimized stacking configuration, long-lived charges with high mobility are detected due to the spatially separated electron/hole transporting π-column, which favors the charge extraction process. However, it is overshadowed by the short-lived singlet states, which hampers the exciton diffusion. Since the main dissociation process, namely EEA, subsequently follows this process, a longer singlet state lifetime is much preferred, which necessitates controlled domain sizes and high crystallinity profile. Pore and skeleton properties are highly correlated which can be tuned through adopting conjugated building blocks and post-synthetic modification. Uniform pore sizes and permanent porosity are also premises for effective exciton diffusion. High dimensionality is indeed promising in forming ohmic contact *via* multiple charge transport pathways, but the synthetic control and steric hindrance need to be well adjusted to suppress charge recombination. For interfacial properties, research has found its relevance to crystallinity and solubility, for which a holistic understanding of planarity, bond stretching and rotations is indispensable.

Even though POP generally boasts of its great absorption extending to the NIR region, the overall low EQE drastically compromises the PCE. This suggests charge dissociation may play a key role. Revisiting the nature of EEA, the energy transfer between two excitons is necessarily an energy cannibalizing process, in which only half of the excited species will progress to the next charge dynamic phase. The aforementioned short diffusion length in COF even further aggrandizes the localization and self-annihilation. Since EEA is excited-state-density sensitive, this rules out its possibility for indoor application. Therefore, employing COF as the main photoactive component may face severe challenges to achieving promising results.

For those PVs exploiting the host–guest structure of COF, several key concerns need to be addressed for achieving high-efficiency devices. Since the main photophysical process shares vast similarities with the conventional D–A bulk heterojunction solar cell, the dissociation efficiency can be engineered by adjusting the driving force. Further insights from excited-state dynamics and charge behavior (*i.e.*, exciton splitting efficiency) are therefore necessary. By performing multi-objective modeling,[178] optimized energy levels and simultaneous increment in overall device performance can be realized. However, the microfabrication technique to incorporate the desired guest molecule remains a challenge. Vapor deposition of C_{60} is most commonly reported, but the incorporation of highly promising polymers as well as emerging small molecules may require advanced techniques to retain the guests inside the framework and adjust interfacial properties.

The unique dynamics between the pore and skeleton design of POP render numerous building blocks and topologies, thus potentially providing endless opportunities for engineering

towards high-efficiency solar cells. As thrilling tectons, synthetic methods, and emerging material are added into the complex, the commensurate boost in solar cell efficiency is yet to come. This indeed indicates the necessity to reveal the fundamental photophysical processes. With regard to the limited number of publications successfully implementing POP as the photoactive component, even fewer directly pinpointed the correlation of the POP structure with the observed charge dynamics and energy losses. Admittedly, the characterization of common POPs remains a formidable challenge due to the rigidity and insolubility issues, which largely restrains the investigation on crystalline COFs. Nevertheless, it still took more than a decade to fully unravel the full photophysical process and underlying mechanism since COF was first invented, and the method to precisely probe the charge yield through EEA is yet reported. Compared to traditional linear polymer characterization where the film investigation directly represents its device component behavior, POPs experimentally more heavily rely on powder. Upon polycondensation, several reports have pointed out the structural variation for solid-state POP in films due to stacking and steric hindrance. Thus, bridging the gap between experiment samples and photoactive components is urgent for effectively controlling the photophysical property. Fortunately, with increased computing power and available molecular models, versatile DFT calculations can help reconstruct the intra- and inter-molecular interaction at an atomic level. With existing knowledge concerning monomers and side groups, the actual molecular orientation and energetic behavior can be predicted. Therefore, it can provide a more molecular-level perspective to interpret characterization results and facilitate chemists to produce much more customized and precise polymers with desired electronic properties.

Regarding computer-aided approaches, multiple machine learning techniques have been employed to optimize the perovskite material combinations. A similar approach can also be extended to POPs to construct a highly conjugated structure for effective charge delocalization. On the other hand, with advanced signal processing techniques, it might be a potential approach to address the poor optical spectral features obtained from POPs. For instance, specific TAS features may be distinguishable to promote more excited dynamics studies.

To improve the commercial attractiveness of POPs, a different approach should be adopted. As opposed to solely improving PCE, the long-term stability and structural advantage can be further explored. Multiple research studies have reported the positive encapsulation effect through the incorporation of rigid POP, which suggests the necessity for extensive degradation. Recent advances in understanding the thermal/photo-degradation with ambient species (O_2/H_2O), thermodynamic related degradation, as well as triplet states impact on stability highlighted the molecular origin of this process.[179–185] Future molecular design and syntheses necessitates more precise control and analyses of molecular vibration, bond strain and twisting, and intermolecular packing. In the meantime, the amorphous feature of most POPs could also be engineered for specific applications. For instance, the intimate and uniform coverage over perovskite promotes its crystallinity, and the high surface area as a counter-electrode translates to higher catalytic events in DSSC. Recent reports highlighted the device incorporation of solution-processable POPs, which indicates the possibility of facile fabrication techniques.

In summary, we have identified the emergence of POPs as a HTL/ETL, and the inclining trend to employ POPs as the main photoactive component. While their great surface passivation and charge transport show great compatibility with PSCs, the hydrophobicity, surface area-enhance catalytic activity, and long-term stability demonstrates POP's potential as electrodes and an electrolyte for DSSCs. In general, more systematic structure-specific photophysical studies need to relate POP properties with charge dynamics and energetics for better device-level implementation. For amorphous POPs, more versatile, cheap, and facile processing and engineering techniques need to be explored to propel their development. With a proportionally increasing number of reports on simulation, characterization, emerging materials, and structures, as well as processing techniques, further efforts can potentially lead to stable enhancement of device performance in the foreseeable future.

Conflicts of interest

There are no conflicts to declare.

References

1 C. Sarkar, S. C. Shit, N. Das and J. Mondal, *Chem. Commun.*, 2021, **57**, 8550–8567.
2 M. Yu, X. Wang, X. Yang, Y. Zhao and J.-X. Jiang, *Polym. Chem.*, 2015, **6**, 3217–3223.
3 Y. Xu, D. Chang, S. Feng, C. Zhang and J.-X. Jiang, *New J. Chem.*, 2016, **40**, 9415–9423.
4 Y. Zhu, Y.-J. Ji, D.-G. Wang, Y. Zhang, H. Tang, X.-R. Jia, M. Song, G. Yu and G.-C. Kuang, *J. Mater. Chem. A*, 2017, **5**, 6622–6629.
5 Y. Li, S. Bi, F. Liu, S. Wu, J. Hu, L. Wang, H. Liu and Y. Hu, *J. Mater. Chem. C*, 2015, **3**, 6876–6881.
6 D. Chen, C. Liu, J. Tang, L. Luo and G. Yu, *Polym. Chem.*, 2019, **10**, 1168–1181.
7 S. Bandyopadhyay, P. Pallavi, A. G. Anil and A. Patra, *Polym. Chem.*, 2015, **6**, 3775–3780.
8 C. Xu, W. Zhang, J. Tang, C. Pan and G. Yu, *Front. Chem.*, 2018, **6**, 592.
9 T. Zhang, G. Xing, W. Chen and L. Chen, *Mater. Chem. Front.*, 2020, **4**, 332–353.
10 S. Bandyopadhyay, A. G. Anil, A. James and A. Patra, *ACS Appl. Mater. Interfaces*, 2016, **8**, 27669–27678.
11 S. Bandyopadhyay, C. Singh, P. Jash, M. D.-W. Hussain, A. Paul and A. Patra, *Chem. Commun.*, 2018, **54**, 6796–6799.
12 X. Liu, C. F. Liu, W. Y. Lai and W. Huang, *Adv. Mater. Technol.*, 2020, 2000154.
13 J. Li, Z. Cheng, M. Zhu, A. Thomas and Y. Liao, *ACS Appl. Energy Mater.*, 2018, **1**, 6535–6540.

14 Z. Xu, L. Hu, J. Ming, X. Cui, M. Zhang, J. Dou, W. Zhang and B. Zhou, *Microporous Mesoporous Mater.*, 2020, **303**, 110259.
15 N. Singh, S. Son, J. An, I. Kim, M. Choi, N. Kong, W. Tao and J. S. Kim, *Chem. Soc. Rev.*, 2021, **50**, 12883–12896.
16 Z. Li and Y. W. Yang, *J. Mater. Chem. B*, 2017, **5**, 9278–9290.
17 Z. Kahveci, A. K. Sekizkardes, R. K. Arvapally, L. Wilder and H. M. El-Kaderi, *Polym. Chem.*, 2017, **8**, 2509–2515.
18 S. Wu, S. Gu, A. Zhang, G. Yu, Z. Wang, J. Jian and C. Pan, *J. Mater. Chem. A*, 2015, **3**, 878–885.
19 F. Song, H. Zhang, D.-G. Wang, T. Chen, S. Yang and G.-C. Kuang, *J. Polym. Sci., Part A: Polym. Chem.*, 2018, **56**, 319–327.
20 P. Jagadesan, G. Eder and P. L. McGrier, *J. Mater. Chem. C*, 2017, **5**, 5676–5679.
21 W. Chen, P. Chen, G. Zhang, G. Xing, Y. Feng, Y. W. Yang and L. Chen, *Chem. Soc. Rev.*, 2021, **50**, 11684–11714.
22 S. Wang, M. Xu, T. Peng, C. Zhang, T. Li, I. Hussain, J. Wang and B. Tan, *Nat. Commun.*, 2019, **10**, 676.
23 J.-S. M. Lee and A. I. Cooper, *Chem. Rev.*, 2020, **120**, 2171–2214.
24 T. Ben, H. Ren, S. Ma, D. Cao, J. Lan, X. Jing, W. Wang, J. Xu, F. Deng, J. M. Simmons, S. Qiu and G. Zhu, *Angew. Chem., Int. Ed.*, 2009, **48**, 9457–9460.
25 P. M. Budd, E. S. Elabas, B. S. Ghanem, S. Makhseed, N. B. McKeown, K. J. Msayib, C. E. Tattershall and D. Wang, *Adv. Mater.*, 2004, **16**, 456–459.
26 K. Geng, T. He, R. Liu, S. Dalapati, K. T. Tan, Z. Li, S. Tao, Y. Gong, Q. Jiang and D. Jiang, *Chem. Rev.*, 2020, **120**, 8814–8933.
27 H. Ding, A. Mal and C. Wang, *Mater. Chem. Front.*, 2020, **4**, 113–127.
28 D. W. Kang, M. Kang and C. S. Hong, *J. Mater. Chem. A*, 2020, **8**, 7474–7494.
29 J. L. Segura, S. Royuela and M. Mar Ramos, *Chem. Soc. Rev.*, 2019, **48**, 3903–3945.
30 T. Ratvijitvech, R. Dawson, A. Laybourn, Y. Z. Khimyak, D. J. Adams and A. I. Cooper, *Polymer*, 2014, **55**, 321–325.
31 H. Bildirir, V. G. Gregoriou, A. Avgeropoulos, U. Scherf and C. L. Chochos, *Mater. Horiz.*, 2017, **4**, 546–556.
32 H. Bildirir, D. Di Carlo Rasi, M. M. Wienk, R. A.-J. Janssen, A. Avgeropoulos, V. G. Gregoriou, S. Allard, U. Scherf and C. L. Chochos, *Macromol. Rapid Commun.*, 2017, **39**, 1700629.
33 J. Zhao, J. Ren, G. Zhang, Z. Zhao, S. Liu, W. Zhang and L. Chen, *Chemistry*, 2021, **27**, 10781–10797.
34 Y. Byun, L. S. Xie, P. Fritz, T. Ashirov, M. Dinca and A. Coskun, *Angew. Chem., Int. Ed.*, 2020, **59**, 15166–15170.
35 W. Zeng, X.-F. Qian, Y.-B. Zhang, J. Yin and Z.-K. Zhu, *Mater. Res. Bull.*, 2005, **40**, 766–772.
36 H. Lu, C. Wang, J. Chen, R. Ge, W. Leng, B. Dong, J. Huang and Y. Gao, *Chem. Commun.*, 2015, **51**, 15562–15565.
37 P. Zhang and S. Dai, *J. Mater. Chem. A*, 2017, **5**, 16118–16127.
38 E. Troschke, S. Grätz, T. Lübken and L. Borchardt, *Angew. Chem., Int. Ed.*, 2017, **56**, 6859–6863.
39 P. Kuhn, M. Antonietti and A. Thomas, *Angew. Chem., Int. Ed.*, 2008, **47**, 3450–3453.
40 J. Maschita, T. Banerjee, G. Savasci, F. Haase, C. Ochsenfeld and B. V. Lotsch, *Angew. Chem., Int. Ed.*, 2020, **59**, 15750–15758.
41 S. Makhseed and J. Samuel, *Chem. Commun.*, 2008, 4342–4344, DOI: **10.1039/b805656k**.
42 C. Monterde, R. Navarro, M. Iglesias and F. Sanchez, *ACS Appl. Mater. Interfaces*, 2019, **11**, 3459–3465.
43 P. Lindemann, M. Tsotsalas, S. Shishatskiy, V. Abetz, P. Krolla-Sidenstein, C. Azucena, L. Monnereau, A. Beyer, A. Gölzhäuser, V. Mugnaini, H. Gliemann, S. Bräse and C. Wöll, *Chem. Mater.*, 2014, **26**, 7189–7193.
44 S. Wuttke, D. D. Medina, J. M. Rotter, S. Begum, T. Stassin, R. Ameloot, M. Oschatz and M. Tsotsalas, *Adv. Funct. Mater.*, 2018, **28**, 1801545.
45 D. D. Medina, J. M. Rotter, Y. Hu, M. Dogru, V. Werner, F. Auras, J. T. Markiewicz, P. Knochel and T. Bein, *J. Am. Chem. Soc.*, 2015, **137**, 1016–1019.
46 Y. Liu, Y. Wang, H. Li, X. Guan, L. Zhu, M. Xue, Y. Yan, V. Valtchev, S. Qiu and Q. Fang, *Chem. Sci.*, 2019, **10**, 10815–10820.
47 K. Dey, M. Pal, K. C. Rout, S. H. Kunjattu, A. Das, R. Mukherjee, U. K. Kharul and R. Banerjee, *J. Am. Chem. Soc.*, 2017, **139**, 13083–13091.
48 H. Liu, Y. Wang, W. Mo, H. Tang, Z. Cheng, Y. Chen, S. Zhang, H. Ma, B. Li and X. Li, *Adv. Funct. Mater.*, 2020, **30**, 1910275.
49 R. Ghosh and F. Paesani, *Chem. Sci.*, 2021, **12**, 8373–8384.
50 Z. Liu, Y. Yin, M. Eginligil, L. Wang, J. Liu and W. Huang, *Polym. Chem.*, 2021, **12**, 807–821.
51 M. Liu, L. Guo, S. Jin and B. Tan, *J. Mater. Chem. A*, 2019, **7**, 5153–5172.
52 R. Liu, K. T. Tan, Y. Gong, Y. Chen, Z. Li, S. Xie, T. He, Z. Lu, H. Yang and D. Jiang, *Chem. Soc. Rev.*, 2021, **50**, 120–242.
53 J. Tan, W.-J. Chen and J. Guo, *Chin. Chem. Lett.*, 2016, **27**, 1405–1411.
54 J. Jeong, M. Kim, J. Seo, H. Lu, P. Ahlawat, A. Mishra, Y. Yang, M. A. Hope, F. T. Eickemeyer, M. Kim, Y. J. Yoon, I. W. Choi, B. P. Darwich, S. J. Choi, Y. Jo, J. H. Lee, B. Walker, S. M. Zakeeruddin, L. Emsley, U. Rothlisberger, A. Hagfeldt, D. S. Kim, M. Gratzel and J. Y. Kim, *Nature*, 2021, **592**, 381–385.
55 NREL, **https://www.nrel.gov/pv/cell-efficiency.html**, 2021.
56 Y. Hu, F. Bai, X. Liu, Q. Ji, X. Miao, T. Qiu and S. Zhang, *ACS Energy Lett.*, 2017, **2**, 2219–2227.
57 F. Jiang, D. Yang, Y. Jiang, T. Liu, X. Zhao, Y. Ming, B. Luo, F. Qin, J. Fan, H. Han, L. Zhang and Y. Zhou, *J. Am. Chem. Soc.*, 2018, **140**, 1019–1027.
58 Y. Cui, Y. Xu, H. Yao, P. Bi, L. Hong, J. Zhang, Y. Zu, T. Zhang, J. Qin, J. Ren, Z. Chen, C. He, X. Hao, Z. Wei and J. Hou, *Adv. Mater.*, 2021, **33**, e2102420.
59 S. Venkatesan, I. P. Liu, C.-M. Tseng Shan, H. Teng and Y.-L. Lee, *Chem. Eng. J.*, 2020, **394**, 124954.
60 M. Chandra Sil, L.-S. Chen, C.-W. Lai, Y.-H. Lee, C.-C. Chang and C.-M. Chen, *J. Power Sources*, 2020, **479**, 229095.
61 D. Devadiga, M. Selvakumar, P. Shetty and M. S. Santosh, *J. Electron. Mater.*, 2021, **50**, 3187–3206.

62 M. Dogru, M. Handloser, F. Auras, T. Kunz, D. Medina, A. Hartschuh, P. Knochel and T. Bein, *Angew. Chem., Int. Ed.*, 2013, **52**, 2920–2924.
63 C. Gu, N. Huang, Y. Chen, H. Zhang, S. Zhang, F. Li, Y. Ma and D. Jiang, *Angew. Chem., Int. Ed.*, 2016, **55**, 3049–3053.
64 S. Yang, C. Yang, X. Zhang, Z. Zheng, S. Bi, Y. Zhang and H. Zhou, *J. Mater. Chem. C*, 2018, **6**, 9044–9048.
65 Y. Li, X. Sun, X. Zhang, D. Zhang, H. Xia, J. Zhou, N. Ahmad, X. Leng, S. Yang, Y. Zhang, Z. A. Li and H. Zhou, *J. Mater. Chem. C*, 2020, **8**, 2676–2681.
66 N. Huang, P. Wang and D. Jiang, *Nat. Rev. Mater.*, 2016, **1**, 16068.
67 X. Chen, M. Addicoat, S. Irle, A. Nagai and D. Jiang, *J. Am. Chem. Soc.*, 2013, **135**, 546–549.
68 F. J. Uribe-Romo, J. R. Hunt, H. Furukawa, C. Klöck, M. O'Keeffe and O. M. Yaghi, *J. Am. Chem. Soc.*, 2009, **131**, 4570–4571.
69 Q. Fang, S. Gu, J. Zheng, Z. Zhuang, S. Qiu and Y. Yan, *Angew. Chem., Int. Ed.*, 2014, **53**, 2878–2882.
70 Y. Meng, Y. Luo, J. L. Shi, H. Ding, X. Lang, W. Chen, A. Zheng, J. Sun and C. Wang, *Angew. Chem., Int. Ed.*, 2020, **59**, 3624–3629.
71 Y. Yang, L. Feng, J. Ren, Y. Liu, S. Jin, L. Su, C. Wood and B. Tan, *Macromol. Rapid Commun.*, 2018, **39**, e1800441.
72 P. Zhang, M. Li, B. Yang, Y. Fang, X. Jiang, G. M. Veith, X. G. Sun and S. Dai, *Adv. Mater.*, 2015, **27**, 8088–8094.
73 S. Luo, Z. Zeng, H. Wang, W. Xiong, B. Song, C. Zhou, A. Duan, X. Tan, Q. He, G. Zeng, Z. Liu and R. Xiao, *Prog. Polym. Sci.*, 2021, **115**, 101374.
74 R. Gao, G. Zhang, F. Lu, L. Chen and Y. Li, *Front. Chem.*, 2021, **9**, 687183.
75 R. K. Sharma, P. Yadav, M. Yadav, R. Gupta, P. Rana, A. Srivastava, R. Zbořil, R. S. Varma, M. Antonietti and M. B. Gawande, *Mater. Horiz.*, 2020, **7**, 411–454.
76 T. Ben and S. Qiu, *CrystEngComm*, 2013, **15**, 17–26.
77 Y. Yuan, Y. Yang and G. Zhu, *EnergyChem*, 2020, **2**, 100037.
78 C. Gu, Y. Chen, Z. Zhang, S. Xue, S. Sun, K. Zhang, C. Zhong, H. Zhang, Y. Pan, Y. Lv, Y. Yang, F. Li, S. Zhang, F. Huang and Y. Ma, *Adv. Mater.*, 2013, **25**, 3443–3448.
79 C. Gu, N. Huang, Y. Chen, L. Qin, H. Xu, S. Zhang, F. Li, Y. Ma and D. Jiang, *Angew. Chem., Int. Ed.*, 2015, **54**, 13594–13598.
80 J. Zhang, S. Xie, X. Zhang, Z. Lu, H. Xiao, C. Li, G. Li, X. Xu, X. Chen and Z. Bo, *Chem. Commun.*, 2017, **53**, 537–540.
81 C. Liu, H. Luo, G. Shi, L. Nian, Z. Chi and Y. Ma, *Dyes Pigm.*, 2017, **142**, 132–138.
82 Q. Fu, T. Wang, Y. Sun, N. Zheng, Z. Xie, D. Lu, Z. Xu, X. Wan, Y. Zhang and Y. Liu, *Sci. China: Chem.*, 2020, **64**, 82–91.
83 Y. Yue, T. Umeyama, Y. Kohara, H. Kashio, M. Itoh, S. Ito, E. Sivaniah and H. Imahori, *J. Phys. Chem. C*, 2015, **119**, 22847–22854.
84 Y. Wang, S. Zhang, J. Wu, K. Liu, D. Li, Q. Meng and G. Zhu, *ACS Appl. Mater. Interfaces*, 2017, **9**, 43688–43695.
85 Z. Zhou, Y. Zhao, C. Zhang, D. Zou, Y. Chen, Z. Lin, H. Zhen and Q. Ling, *J. Mater. Chem. A*, 2017, **5**, 6613–6621.
86 L. Calió, C. Momblona, L. Gil-Escrig, S. Kazim, M. Sessolo, Á. Sastre-Santos, H. J. Bolink and S. Ahmad, *Sol. Energy Mater. Sol. Cells*, 2017, **163**, 237–241.
87 S. Park, M. S. Kim, W. Jang, J. K. Park and D. H. Wang, *Nanoscale*, 2018, **10**, 4708–4717.
88 C. Wu, Y. Liu, H. Liu, C. Duan, Q. Pan, J. Zhu, F. Hu, X. Ma, T. Jiu, Z. Li and Y. Zhao, *J. Am. Chem. Soc.*, 2018, **140**, 10016–10024.
89 Y. Li, Q. Chen, T. Xu, Z. Xie, J. Liu, X. Yu, S. Ma, T. Qin and L. Chen, *J. Am. Chem. Soc.*, 2019, **141**, 13822–13828.
90 J. Lim, M.-S. Kim, W. Jang, D. H. Wang and J. K. Park, *Dyes Pigm.*, 2020, **178**, 108332.
91 M. G. Mohamed, C.-C. Lee, A. F.-M. El-Mahdy, J. Lüder, M.-H. Yu, Z. Li, Z. Zhu, C.-C. Chueh and S.-W. Kuo, *J. Mater. Chem. A*, 2020, **8**, 11448–11459.
92 Q. Fu, Z. Xu, X. Tang, T. Liu, X. Dong, X. Zhang, N. Zheng, Z. Xie and Y. Liu, *ACS Energy Lett.*, 2021, 1521–1532, DOI: **10.1021/acsenergylett.1c00385,**.
93 T. C. Wei, C. C. Wan and Y. Y. Wang, *Sol. Energy Mater. Sol. Cells*, 2007, **91**, 1892–1897.
94 X. Zhang, C.-X. Wang, F.-Y. Li and Y.-Y. Xia, *J. Photochem. Photobiol., A*, 2008, **194**, 31–36.
95 C.-M. Chen, H.-S. Shiu, S.-J. Cherng and T.-C. Wei, *J. Power Sources*, 2009, **188**, 319–322.
96 H. Yang, O. A. Ileperuma, M. Shimomura and K. Murakami, *Sol. Energy Mater. Sol. Cells*, 2009, **93**, 1083–1086.
97 S. Ahmad, J. H. Yum, H. J. Butt, M. K. Nazeeruddin and M. Gratzel, *ChemPhys Chem*, 2010, **11**, 2814–2819.
98 S. Ahmad, T. Bessho, F. Kessler, E. Baranoff, J. Frey, C. Yi, M. Gratzel and M. K. Nazeeruddin, *Phys. Chem. Chem. Phys.*, 2012, **14**, 10631–10639.
99 M. Thomas and S. Rajiv, *J. Photochem. Photobiol., A*, 2020, **394**, 112464.
100 L. Chen, K. Furukawa, J. Gao, A. Nagai, T. Nakamura, Y. Dong and D. Jiang, *J. Am. Chem. Soc.*, 2014, **136**, 9806–9809.
101 T. Liu and G. Liu, *Nat. Commun.*, 2020, **11**, 4984.
102 N. C. Flanders, M. S. Kirschner, P. Kim, T. J. Fauvell, A. M. Evans, W. Helweh, A. P. Spencer, R. D. Schaller, W. R. Dichtel and L. X. Chen, *J. Am. Chem. Soc.*, 2020, **142**, 14957–14965.
103 Y. Wang, Y. Liu, H. Li, X. Guan, M. Xue, Y. Yan, V. Valtchev, S. Qiu and Q. Fang, *J. Am. Chem. Soc.*, 2020, **142**, 3736–3741.
104 M. Yang, X. Long, H. Li, H. Chen and P. Liu, *ACS Sustainable Chem. Eng.*, 2018, **7**, 2236–2244.
105 J. Yang, M. Xu, J. Wang, S. Jin and B. Tan, *Sci. Rep.*, 2018, **8**, 4200.
106 S.-L. Cai, Y.-B. Zhang, A. B. Pun, B. He, J. Yang, F. M. Toma, I. D. Sharp, O. M. Yaghi, J. Fan, S.-R. Zheng, W.-G. Zhang and Y. Liu, *Chem. Sci.*, 2014, **5**, 4693–4700.
107 H. Ding, Y. Li, H. Hu, Y. Sun, J. Wang, C. Wang, C. Wang, G. Zhang, B. Wang, W. Xu and D. Zhang, *Chemistry*, 2014, **20**, 14614–14618.
108 H. Li, H. Li, S. Xun and J.-L. Brédas, *Chem. Mater.*, 2020, **32**, 9228–9237.

109 D. W. Kang, J. H. Song, K. J. Lee, H. G. Lee, J. E. Kim, H. Y. Lee, J. Y. Kim and C. S. Hong, *J. Mater. Chem. A*, 2017, **5**, 17492–17498.
110 J. Kim, *Pure Appl. Chem.*, 2002, **74**, 2031–2044.
111 Z. Luo, C. Sun, S. Chen, Z.-G. Zhang, K. Wu, B. Qiu, C. Yang, Y. Li and C. Yang, *Adv. Energy Mater.*, 2018, **8**, 1800856.
112 G. Zeng, Y. Xin, B. Zhang, J. Ouyang, X. Zhao and X. Yang, *Sol. RRL*, 2020, **4**, 2000234.
113 G. Ding, Y. Wu, Y. Weng, W. Zhang and Z. Hu, *Macromolecules*, 2013, **46**, 8638–8643.
114 S. Osawa, T. Ogawa and M. Ito, *Synth. Met.*, 1997, **90**, 109–113.
115 J. Genzer, E. Sivaniah, E. J. Kramer, J. Wang, H. Körner, K. Char, C. K. Ober, B. M. DeKoven, R. A. Bubeck, D. A. Fischer and S. Sambasivan, *Langmuir*, 2000, **16**, 1993–1997.
116 S. Jin, M. Supur, M. Addicoat, K. Furukawa, L. Chen, T. Nakamura, S. Fukuzumi, S. Irle and D. Jiang, *J. Am. Chem. Soc.*, 2015, **137**, 7817–7827.
117 A. Mahringer and D. D. Medina, *Nat. Chem.*, 2020, **12**, 985–987.
118 X. Ding, L. Chen, Y. Honsho, X. Feng, O. Saengsawang, J. Guo, A. Saeki, S. Seki, S. Irle, S. Nagase, V. Parasuk and D. Jiang, *J. Am. Chem. Soc.*, 2011, **133**, 14510–14513.
119 J. R. Tumbleston, B. A. Collins, L. Yang, A. C. Stuart, E. Gann, W. Ma, W. You and H. Ade, *Nat. Photonics*, 2014, **8**, 385–391.
120 F. Auras, L. Ascherl, A. H. Hakimioun, J. T. Margraf, F. C. Hanusch, S. Reuter, D. Bessinger, M. Doblinger, C. Hettstedt, K. Karaghiosoff, S. Herbert, P. Knochel, T. Clark and T. Bein, *J. Am. Chem. Soc.*, 2016, **138**, 16703–16710.
121 L. Ascherl, T. Sick, J. T. Margraf, S. H. Lapidus, M. Calik, C. Hettstedt, K. Karaghiosoff, M. Döblinger, T. Clark, K. W. Chapman, F. Auras and T. Bein, *Nat. Chem.*, 2016, **8**, 310–316.
122 L. Ye, S. Li, X. Liu, S. Zhang, M. Ghasemi, Y. Xiong, J. Hou and H. Ade, *Joule*, 2019, **3**, 443–458.
123 L. Li, W.-y Lo, Z. Cai, N. Zhang and L. Yu, *Macromolecules*, 2016, **49**, 6903–6909.
124 V. S. Mothika, P. Sutar, P. Verma, S. Das, S. K. Pati and T. K. Maji, *Chemistry*, 2019, **25**, 3867–3874.
125 T. Li, W. Zhu, R. Shen, H.-Y. Wang, W. Chen, S.-J. Hao, Y. Li, Z.-G. Gu and Z. Li, *New J. Chem.*, 2018, **42**, 6247–6255.
126 Z. Liu, X. Yuan, S. Zhang, J. Wang, Q. Huang, N. Yu, Y. Zhu, L. Fu, F. Wang, Y. Chen and Y. Wu, *NPG Asia Mater.*, 2019, **11**, 12.
127 S. Bracco, D. Piga, I. Bassanetti, J. Perego, A. Comotti and P. Sozzani, *J. Mater. Chem. A*, 2017, **5**, 10328–10337.
128 A. Giri, A. Sahoo, T. K. Dutta and A. Patra, *ACS Omega*, 2020, **5**, 28413–28424.
129 P. W. Fritz and A. Coskun, *Chemistry*, 2021, **27**, 7489–7501.
130 Y. Xie, J. Li, C. Lin, B. Gui, C. Ji, D. Yuan, J. Sun and C. Wang, *J. Am. Chem. Soc.*, 2021, **143**, 7279–7284.
131 H. Li, J. Li, A. Thomas and Y. Liao, *Adv. Funct. Mater.*, 2019, **29**, 1904785.
132 A. Modak, J. Mondal and A. Bhaumik, *Appl. Catal., A*, 2013, **459**, 41–51.
133 B. C. Patra, S. Khilari, L. Satyanarayana, D. Pradhan and A. Bhaumik, *Chem. Commun.*, 2016, **52**, 7592–7595.
134 Y. Xia, Y. Li, Y. Gu, T. Jin, Q. Yang, J. Hu, H. Liu and H. Wang, *Fuel*, 2016, **170**, 100–106.
135 V. Coropceanu, X.-K. Chen, T. Wang, Z. Zheng and J.-L. Brédas, *Nat. Rev. Mater.*, 2019, **4**, 689–707.
136 J. Yan, E. Rezasoltani, M. Azzouzi, F. Eisner and J. Nelson, *Nat. Commun.*, 2021, **12**, 3642.
137 F. D. Eisner, M. Azzouzi, Z. Fei, X. Hou, T. D. Anthopoulos, T. J.-S. Dennis, M. Heeney and J. Nelson, *J. Am. Chem. Soc.*, 2019, **141**, 6362–6374.
138 Z. Wen, T. Wang, Z. Chen, T. Jiang, L. Feng, X. Feng, C. Qin and X. Hao, *Chin. Chem. Lett.*, 2021, **32**, 529–534.
139 N. Yao, J. Wang, Z. Chen, Q. Bian, Y. Xia, R. Zhang, J. Zhang, L. Qin, H. Zhu, Y. Zhang and F. Zhang, *J. Phys. Chem. Lett.*, 2021, **12**, 5039–5044.
140 N. Gasparini, A. Salleo, I. McCulloch and D. Baran, *Nat. Rev. Mater.*, 2019, **4**, 229–242.
141 S. Karuthedath, J. Gorenflot, Y. Firdaus, N. Chaturvedi, C. S.-P. De Castro, G. T. Harrison, J. I. Khan, A. Markina, A. H. Balawi, T. A.-D. Pena, W. Liu, R. Z. Liang, A. Sharma, S. H.-K. Paleti, W. Zhang, Y. Lin, E. Alarousu, D. H. Anjum, P. M. Beaujuge, S. De Wolf, I. McCulloch, T. D. Anthopoulos, D. Baran, D. Andrienko and F. Laquai, *Nat. Mater.*, 2021, **20**, 378–384.
142 M. Schwarze, K. S. Schellhammer, K. Ortstein, J. Benduhn, C. Gaul, A. Hinderhofer, L. Perdigon Toro, R. Scholz, J. Kublitski, S. Roland, M. Lau, C. Poelking, D. Andrienko, G. Cuniberti, F. Schreiber, D. Neher, K. Vandewal, F. Ortmann and K. Leo, *Nat. Commun.*, 2019, **10**, 2466.
143 N. Gasparini, F. V.-A. Camargo, S. Fruhwald, T. Nagahara, A. Classen, S. Roland, A. Wadsworth, V. G. Gregoriou, C. L. Chochos, D. Neher, M. Salvador, D. Baran, I. McCulloch, A. Gorling, L. Luer, G. Cerullo and C. J. Brabec, *Nat. Commun.*, 2021, **12**, 1772.
144 I. Castano, A. M. Evans, R. D. Reis, V. P. Dravid, N. C. Gianneschi and W. R. Dichtel, *Chem. Mater.*, 2021, **33**, 1341–1352.
145 A. M. Evans, I. Castano, A. Brumberg, L. R. Parent, A. R. Corcos, R. L. Li, N. C. Flanders, D. J. Gosztola, N. C. Gianneschi, R. D. Schaller and W. R. Dichtel, *J. Am. Chem. Soc.*, 2019, **141**, 19728–19735.
146 M. Evans Austin, R. Parent Lucas, C. Flanders Nathan, P. Bisbey Ryan, E. Vitaku, S. Kirschner Matthew, D. Schaller Richard, X. Chen Lin, C. Gianneschi Nathan and R. Dichtel William, *Science*, 2018, **361**, 52–57.
147 S. Jin, X. Ding, X. Feng, M. Supur, K. Furukawa, S. Takahashi, M. Addicoat, M. E. El-Khouly, T. Nakamura, S. Irle, S. Fukuzumi, A. Nagai and D. Jiang, *Angew. Chem., Int. Ed.*, 2013, **52**, 2017–2021.
148 A. C. Jakowetz, T. F. Hinrichsen, L. Ascherl, T. Sick, M. Calik, F. Auras, D. D. Medina, R. H. Friend, A. Rao and T. Bein, *J. Am. Chem. Soc.*, 2019, **141**, 11565–11571.

149 T. W. Kim, S. Jun, Y. Ha, R. K. Yadav, A. Kumar, C. Y. Yoo, I. Oh, H. K. Lim, J. W. Shin, R. Ryoo, H. Kim, J. Kim, J. O. Baeg and H. Ihee, *Nat. Commun.*, 2019, **10**, 1873.
150 K. V. Rao, R. Haldar, T. K. Maji and S. J. George, *Phys. Chem. Chem. Phys.*, 2016, **18**, 156–163.
151 E. Rephaeli and S. Fan, *Opt. Express*, 2009, **17**, 15145–15159.
152 Y. Z. Peng, G. C. Guo, S. Guo, L. H. Kong, T. B. Lu and Z. M. Zhang, *Angew. Chem., Int. Ed.*, 2021, **60**, 22062–22069.
153 V. Gray, D. Dzebo, M. Abrahamsson, B. Albinsson and K. Moth-Poulsen, *Phys. Chem. Chem. Phys.*, 2014, **16**, 10345–10352.
154 L. Yao, Y. Zhang, H.-X. Wang, Y. Guo, Z.-M. Zhuang, W. Wen, X. Zhang and S. Wang, *J. Mater. Chem. A*, 2020, **8**, 8518–8526.
155 B. Xu, S. Li, H. Jiao, J. Yin, Z. Liu and W. Zhong, *J. Mater. Chem. A*, 2020, **8**, 3865–3871.
156 S. Dong, T. Jia, K. Zhang, J. Jing and F. Huang, *Joule*, 2020, **4**, 2004–2016.
157 J. K. Tan, R. Q. Png, C. Zhao and P. K.-H. Ho, *Nat. Commun.*, 2018, **9**, 3269.
158 X. Song, N. Gasparini and D. Baran, *Adv. Electron. Mater.*, 2018, **4**, 1700358.
159 Z. Zheng, Q. Hu, S. Zhang, D. Zhang, J. Wang, S. Xie, R. Wang, Y. Qin, W. Li, L. Hong, N. Liang, F. Liu, Y. Zhang, Z. Wei, Z. Tang, T. P. Russell, J. Hou and H. Zhou, *Adv. Mater.*, 2018, e1801801, DOI: **10.1002/adma.201801801**.
160 S. Yu, B. Guo, S. Johnsen, G. Wiegand, U. Lemmer, X. Guo, M. Zhang, Y. Li, C. Sprau, H. Hölscher, A. Colsmann and G. Gomard, *Energy Technol.*, 2021, **10**, 2100676.
161 T. Wu, Z. Qin, Y. Wang, Y. Wu, W. Chen, S. Zhang, M. Cai, S. Dai, J. Zhang, J. Liu, Z. Zhou, X. Liu, H. Segawa, H. Tan, Q. Tang, J. Fang, Y. Li, L. Ding, Z. Ning, Y. Qi, Y. Zhang and L. Han, *Nanomicro Lett.*, 2021, **13**, 152.
162 M. A. Green, A. Ho-Baillie and H. J. Snaith, *Nat. Photonics*, 2014, **8**, 506–514.
163 N. Suresh Kumar and K. Chandra Babu Naidu, *J. Materiomics*, 2021, **7**, 940–956.
164 N. Ali, N. Shehzad, S. Uddin, R. Ahmed, M. Jabeen, A. Kalam, A. G. Al-Sehemi, H. Alrobei, M. B. Kanoun, A. Khesro and S. Goumri-Said, *Int. J. Energy Res.*, 2021, **45**, 19729–19745.
165 J. Y. Kim, J.-W. Lee, H. S. Jung, H. Shin and N.-G. Park, *Chem. Rev.*, 2020, **120**, 7867–7918.
166 H. J. Snaith, *J. Phys. Chem. Lett.*, 2013, **4**, 3623–3630.
167 G. Hodes and D. Cahen, *Nat. Photonics*, 2014, **8**, 87–88.
168 C. Huang, S. Barlow and S. R. Marder, *J. Org. Chem.*, 2011, **76**, 2386–2407.
169 B. O'Regan and M. Grätzel, *Nature*, 1991, **353**, 737–740.
170 S. Shalini, R. Balasundaraprabhu, T. S. Kumar, N. Prabavathy, S. Senthilarasu and S. Prasanna, *Int. J. Energy Res.*, 2016, **40**, 1303–1320.
171 V. Sugathan, E. John and K. Sudhakar, *Renewable Sustainable Energy Rev.*, 2015, **52**, 54–64.
172 M. Shakeel Ahmad, A. K. Pandey and N. Abd Rahim, *Renewable Sustainable Energy Rev.*, 2017, **77**, 89–108.
173 N. Yan, C. Zhao, S. You, Y. Zhang and W. Li, *Chin. Chem. Lett.*, 2020, **31**, 643–653.
174 J. Gong, J. Liang and K. Sumathy, *Renewable Sustainable Energy Rev.*, 2012, **16**, 5848–5860.
175 K. Sharma, V. Sharma and S. S. Sharma, *Nanoscale Res. Lett.*, 2018, **13**, 381.
176 C.-M. Shih, Y.-L. Wu, Y.-C. Wang, S. R. Kumar, Y.-L. Tung, C.-C. Yang and S. J. Lue, *J. Photochem. Photobiol., A*, 2018, **356**, 565–572.
177 Q. Li, J. Wu, Q. Tang, Z. Lan, P. Li, J. Lin and L. Fan, *Electrochem. Commun.*, 2008, **10**, 1299–1302.
178 N. Gasparini, F. V.-A. Camargo, S. Frühwald, T. Nagahara, A. Classen, S. Roland, A. Wadsworth, V. G. Gregoriou, C. L. Chochos, D. Neher, M. Salvador, D. Baran, I. McCulloch, A. Görling, L. Lüer, G. Cerullo and C. J. Brabec, *Nat. Commun.*, 2021, **12**, 1772.
179 I. Ramirez, A. Privitera, S. Karuthedath, A. Jungbluth, J. Benduhn, A. Sperlich, D. Spoltore, K. Vandewal, F. Laquai and M. Riede, *Nat. Commun.*, 2021, **12**, 471.
180 Y. Zhu, A. Gadisa, Z. Peng, M. Ghasemi, L. Ye, Z. Xu, S. Zhao and H. Ade, *Adv. Energy Mater.*, 2019, **9**, 1900376.
181 N. A. Tegegne, H. Wendimu, Z. Abdissa, W. Mammo, M. R. Andersson, F. G. Hone, D. M. Andoshee, O. Olaoye and G. Bosman, *J. Mater. Sci.: Mater. Electron.*, 2020, **31**, 21303–21315.
182 M. Ghasemi, H. Hu, Z. Peng, J. J. Rech, I. Angunawela, J. H. Carpenter, S. J. Stuard, A. Wadsworth, I. McCulloch, W. You and H. Ade, *Joule*, 2019, **3**, 1328–1348.
183 K. Kawano, R. Pacios, D. Poplavskyy, J. Nelson, D. D.-C. Bradley and J. R. Durrant, *Sol. Energy Mater. Sol. Cells*, 2006, **90**, 3520–3530.
184 L. Duan, H. Yi, Y. Zhang, F. Haque, C. Xu and A. Uddin, *Sustainable Energy Fuels*, 2019, **3**, 723–735.
185 L. Duan, M. Guli, Y. Zhang, H. Yi, F. Haque and A. Uddin, *Energy Technol.*, 2020, **8**, 1901401.